Eindhoven University of Technology

MASTER

Bed dynamics due to a particle impact

Gäbler, J.

Award date:
2007

Link to publication

Disclaimer
This document contains a student thesis (bachelor's or master's), as authored by a student at Eindhoven University of Technology. Student theses are made available in the TU/e repository upon obtaining the required degree. The grade received is not published on the document as presented in the repository. The required complexity or quality of research of student theses may vary by program, and the required minimum study period may vary in duration.

General rights
Copyright and moral rights for the publications made accessible in the public portal are retained by the authors and/or other copyright owners and it is a condition of accessing publications that users recognise and abide by the legal requirements associated with these rights.

- Users may download and print one copy of any publication from the public portal for the purpose of private study or research.
- You may not further distribute the material or use it for any profit-making activity or commercial gain

BED DYNAMICS DUE TO A PARTICLE IMPACT

J. Gäbler
WET 2007.06

Committee:
prof. dr. ir. A.A. van Steenhoven (chairman)
dr. ir. C.C.M. Rindt (supervisor)
dr.ir. M.S. Abd-Elhady (supervisor)
dr.ir. H.P. van Kemenade
ir. J.G. Wijers

Technische Universiteit Eindhoven
Department of Mechanical Engineering
Division Thermo Fluids Engineering

BED DYNAMICS DUE TO A PARTICLE IMPACT

J. Gäbler

Samenvatting

De efficiëntie van warmte wisselaars wordt negatief beïnvloed door de depositie van vliegas deeltjes op de pijpen van de warmte wisselaar. De depositie van deze deeltjes op de pijpen bundel wordt fouling genoemd. De depositie laag kan zowel poederachtig als gesinterd zijn, afhankelijk van de gas temperatuur. De vliegas deeltjes in de hete gas stroom botsen met de depositie laag en een interactie tussen de deeltjes vindt plaats. In dit onderzoek is de interactie tussen een inkomend deeltje en een bed van deeltjes experimenteel en numeriek onderzocht.

Met behulp van een '3D' opstelling zijn botsingsproeven uitgevoerd op een bed van bronzen micron deeltjes. Met deze experimenten is het gedrag van het inkomende deeltje en de bed deeltjes na de botsing onderzocht voor verschillende inslag snelheden en deeltjes diameters. Deze experimenten laten zien dat er verschillende fenomenen kunnen optreden namelijk plakken of stuiteren van het inkomende deeltje op de bed deeltjes. Wanneer het inkomende deeltje stuitert op de bed deeltjes kunnen er ook deeltjes verwijderd worden uit het bed. De inslag snelheid waarbij er verwijdering plaats vindt, is afhankelijk van de diameter van het inkomende deeltje. Met een toenemende deeltjes diameter, en een gelijkblijvende diameter van de bed deeltjes, zal de snelheid waarbij verwijdering optreedt afnemen. De snelheden waarbij de verschillende fenomenen optreden laten een overlap zien.

Om de bed dynamica in meer detail te onderzoeken is een '2D' opstelling gebouwd waarin experimenten met millimeter deeltjes zijn uitgevoerd. Een inslag van een stalen deeltje op een bed van nylon deeltjes laat zien dat de snelheids ratio van het inkomende deeltje afhankelijk is van de inslag positie en het aantal bed lagen. Een afnemende hoeveelheid bed lagen resulteert in een grotere snelheids ratio. De experimenten laten ook zien dat de uitkomst van de botsing sterk afhankelijk is van de bodem eigenschappen waarop het deeltjes bed is gesitueerd. Met de experimentele opstelling is het ook mogelijk om de contact tijd tussen het inkomende deeltje en het bed deeltje te bepalen.

De resultaten van de 2D experimenten zijn vergeleken met de uitkomst van numerieke simulaties. Het numerieke model is gebaseerd op de discrete elementen methode. De optredende krachten tussen de botsende deeltjes worden beschreven door de contact mechanica. Met de numerieke simulaties is ook de afhankelijkheid van de snelheids ratio op de inslag positie gevonden. De contact tijd tussen het inkomende deeltje en het bed deeltje is berekend met de numerieke simulatie en komt overeen met de contact tijd gevonden in het experiment.

Summary

The efficiency of heat exchangers is negatively influenced by the deposition of fly ash particles on the heat exchanger tubes. The deposition of these particles on the heat exchanger tubes is called fouling. The fouling layer can be powdery or sintered depending on the gas-side temperature. The fly ash particles situated in the hot gas stream collide with the fouling layer and particle interaction takes place. In this research the interaction between an incident particle and a bed of particles is experimentally and numerically investigated.

With a '3D' set-up impacting experiments are performed on a bed of bronze micron particles. With these experiments the post-collision behavior of the incident particle and bed particles is investigated with varying incident velocities and particle diameter. These experiments show that different phenomena can occur namely sticking of the incident particle on the bed of particles or bouncing of the incident particle from the bed of particles. If the incident particle bounces of the bed, particles can also be removed from the bed. The incident velocity at which removal takes place is found to be dependent on the incident particle diameter. With increasing incident particle diameter, and a constant bed particle diameter, the removal velocity decreases. It is also found that the velocity regimes in which one of the post-collision phenomena occur show an overlap.

In order to investigate the bed dynamics in more detail a '2D' set-up was built in which experiments with millimetre particles are performed. Impaction of a steel incident particle on a bed of nylon particles shows that the velocity ratio of the incident particle is dependent on the impact position and the amount of bed layers. With a decreasing amount of bed layers a higher velocity ratio is found. The experiments also show that the outcome of a collision is strongly dependent on the bottom properties on which the bed is situated. With the experimental set-up it is also possible the determine the contact time between the incident particle and the target particle.

The results of the 2D experiments are compared with the outcome of numerical simulations. The numerical model used for the simulation is based on the discrete element method. In this model the contact forces between the interacting particles are based on the concepts of contact mechanics. With the numerical simulations it is also found that the velocity ratio is dependent on the impact position of the incident particle. The contact time between the incident particle and the target particle is determined with the numerical model, from which the force propagation speed could be determined. The contact time found in the experiment corresponds with the contact time found with the numerical simulation.

Nomenclature

Roman

c	calibration constant	-
C_m	mass ratio	-
E	Young's modulus	N/m^2
f_{ch}	chopper frequency	Hz
$\mathbf{F}$	force vector	N
$\mathbf{F}_{adh}$	adhesion force	N
$\mathbf{F}_{cn}$	contact force in normal direction	N
$\mathbf{F}_{ct}$	contact force in tangential direction	N
F_{el}	average elastic force	N
h	distance, height	m
m	mass	kg
$\mathbf{n}$	unit vector in normal direction	-
R	particle radius	m
R_c	particle contact radius	m
$\mathbf{t}$	unit vector in tangential direction	-
v_i	incident velocity	m/s
$v_{i,n}$	impact velocity in normal direction	m/s
$v_{i,el}$	limiting elastic velocity	m/s
$\ddot{\mathbf{x}}$	acceleration vector	m/s^2
$\dot{\mathbf{x}}$	velocity vector	m/s
$\dot{\mathbf{x}}_0$	initial velocity vector	m/s
$\mathbf{x}$	position vector	m
$\mathbf{x}_0$	initial position vector	m
y	elastic load limit	N/m^2

Greek

Δt	time step	s
δ	interpenetration distance	m
δ_{el}	elastic deformation limit	m
δ_p	remnant plastic deformation	m
Γ	surface free energy	J/m^2
μ_k	kinematic friction coefficient	-
ν	Poison ratio	-
ρ	mass density	kg/m^3
σ_y	yield stress	N/m^2
τ	contact time	s

Subscripts

0	initial
1,2	particle number
adh	adhesion
cn	normal contact
ct	tangential contact
el	elastic limit
i	incident,initial
p	plastic
y	yield

Superscript

*	reduced

Contents

Chapter 1

Introduction

The need for energy is as high as ever and the demand for energy is still growing. According to the international energy agency (IEA) the global primary energy demand will increase with 53 percent between now and 2030 [8]. Most of the energy is generated with fossil fuels and a small amount via renewable energy sources. In the proces of generating energy a lot of heat is produced. In order to increase the efficiency the heat can be recovered by placing heat exchangers in the gas stream. In the hot gas stream fly ash particles are present and they deposit on the heat exchanger. The deposition of these particles on the heat exchanger is called fouling and results in an insulating layer on the heat exchanger tubes. Due to this insulating layer the heat transfer coefficient reduces and the efficiency of the heat exchanger decreases. The fouling layer on an heat exchanger can be powdery or sintered, depending on the gas-side temperature. In figure 1.1.a an example of a powdery fouling layer is presented and in figure 1.1.b a sintered layer.

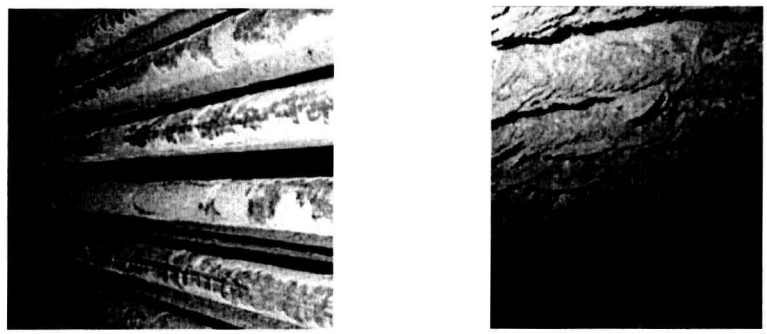

(a) (b)

Figure 1.1: Examples of fouling layers on heat exchanger tubes.
(a) Powdery fouling layer in an economizer.
(b) Sintered fouling layer in a superheater.

The particles in the gas stream collide with the heat exchanger tube and stick to the tube. In time the fouling layer will grow because more particles stick to the tube. This growth appears to show an asymptotic behavior. So in time there is a balance between the amount of removed particles, due to particle impaction, and the amount of particles that stick to the tube.

The ultimate goal in the research field of fouling is to develop a model that can describe the proces of fouling. In this model the gas stream around a cylinder and the transport of particles in the gas stream needs to be calculated. The second step is to check if the particles are colliding with the wall of the tube. If they collide with the wall the interaction between the particle and the wall or between the particle and the fouling layer needs to be determined. The colliding particle can stick to or bounce off the wall or the fouling layer. When the incident particle hits the fouling layer it can remove particles from the fouling layer. When the particle bounces of or when it removes particles they return in the gas stream and can collide again to the heat exchanger tube. In figure 1.2 a schematic view of the fouling proces on a tube is presented.

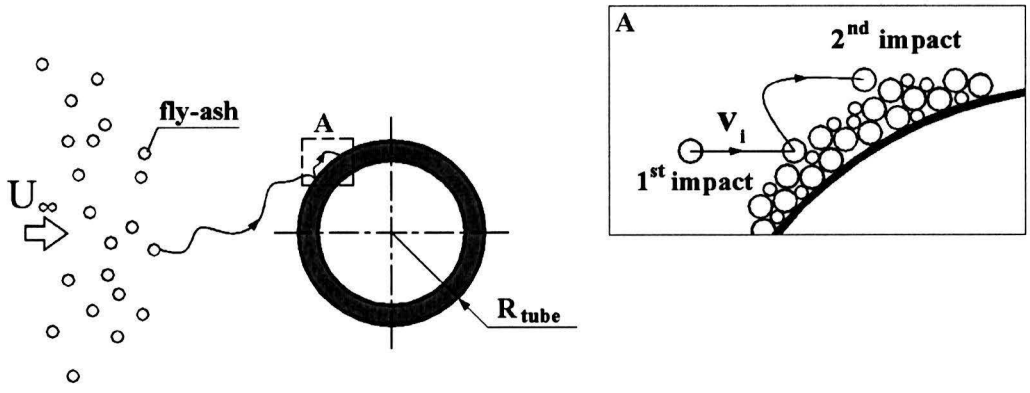

Figure 1.2: Deposition of particulate matter on a tube in a cross flow.

In this research the interaction between an incident particle and a bed of particles is investigated. An overview of several numerical methods that simulate the outcome of a collision between a bed of particles and an incident particle is presented in chapter 2. In order to investigate the bed dynamics due to an impact of an incident particle, impaction experiments are performed. With these experiments the behavior of the incident particle and the bed particles can be followed. For the experiments two different experimental set-ups are used, a 3D set-up and a 2D set-up. With the 3D set-up impacting experiments with bronze micron particles are performed. With these experiments the post-collision behavior of the incident particle and bed particles are investigated with varying incident velocities. In order to investigate the bed dynamics in more detail a 2D set-up was built in which impacting experiments with millimetre particles can be performed. In chapter 3 a description of these experimental set-ups and the experimental results are presented. The interaction of a particle hitting a bed of particles is simulated numerically using the numerical code developed by Abd-Elhady et al. [1]. In these simulations the bed dynamics are investigated for varying incident velocities, bed heights and particle properties. The results of these simulations are compared with the performed 2D experiments. The results of these numerical simulations are presented in chapter 4. In chapter 5 the overall conclusions and recommendations are presented.

Chapter 2

Particle interaction modeling

In literature several models can be found that simulate the outcome of a collision between an incident particle and a bed of particles. In figure 2.1 two examples of a collision between an incident particle and a bed of particles are presented. Figure 2.1.a shows a bronze particle colliding with a powdery bed of bronze particles and figure 2.1.b a steel particle colliding with a bed of nylon particles.

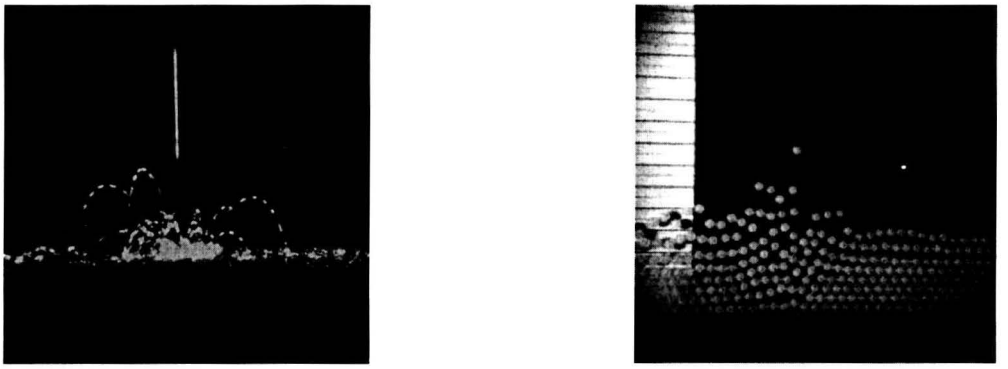

(a) (b)

Figure 2.1: (a) Impaction of a bronze particle on a powdery bed of bronze particles.
(b) Impaction of a steel particle on a bed of nylon particles.

In this chapter three different models are presented that can be used for simulation of the particle interaction. The first model that is presented is the two-body collision model. In this model the interaction between an incident particle and a bed of particles is modeled as a collision between two particles. The second model is a discrete element method based on Newton's second law of motion. In this model the position and velocity of the interacting particles are determined using Newton's second law of motion. The forces that occur between the interacting particles are described by the theory of contact mechanics. The last model that is described is the spring-damper model. The spring-damper model is also a discrete element method in which the forces between the interacting particles are approximated by a spring and a damper model.

2.1 Two-body collision model

In the two-body collision model, as used by van Beek et al. [4], the interaction between an incident particle and a bed of particles is modeled as a collision between two particles. In the model the second body represents the bed of particles which has a mass (m_2) that is proportional to the mass of the incident particle (m_1) according to

$$m_2 = C_m m_1 \tag{2.1}$$

in which C_m is the proportionality factor. The outcome of a two body collision is determined not only by the proportionality factor but also by the coefficient of restitution e and the friction coefficient f. The friction coefficient is the ratio between the contact force in normal and tangential direction and the coefficient of restitution is a measure for energy losses during a collision.

The collision between two particles can be divided into two phases, the approach phase and the restitution phase. The first phase of the collision, the approach phase, starts when the two colliding particles are just in contact with each other. At the beginning of the approach there are no repulsive forces between the two particles. As a result of the relative velocity in normal direction the contact area between the particles deforms and a contact force develops.

Due to the contact forces the incident particle decelerates and the target particle accelerates until the relative velocity of the two particles becomes zero. When the relative velocity of the particles becomes zero the contact force has reached its maximum value and the approach phase ends. The deformation of the particles during the approach phase is elastic or plastic-elastic, when a critical value is exceeded. In the restitution phase the particles are still in contact with each other but the particles start to move away from each other and the contact force reduces to zero.

In the two-body collision model the maximum contact force between the interacting particles is calculated by solving the energy balance that holds at the end of the approach phase. The energy balance for a collision where only elastic deformation of the colliding particles occur reads [4]

$$Q_k + Q_{A,a}(F) = Q_e(F) \tag{2.2}$$

where Q_k is the kinetic energy of the incident particle with an effective mass m^*, $Q_{A,a}$ the surface energy released to the system in the approach phase and Q_e the elastic energy stored in the colliding particles. The effective mass m^* is defined as

$$m^* = \frac{m_1 m_2}{m_1 + m_2} \tag{2.3}$$

When there is also plastic deformation of the colliding particles the energy balance reads

$$Q_k + Q_{A,a}(F) = Q_{el} + Q_{pe}(F) + Q_p(F) \tag{2.4}$$

where Q_{el} is the maximum amount of elastic energy stored in the colliding particles, Q_{pe} the stored elastic energy during plastic deformation and Q_p the dissipated energy during plastic deformation. The energies are dependent on the material properties and on the contact force between the colliding particles. Therefore the only unknown in the energy balance is the contact force F. The different energy relations are given in appendix A. The coefficient of restitution, which is a measure for the energy loss over a collision, is given as [4]

$$e^2 = 1 - \frac{Q_p + (Q_{A,r} - Q_{A,a})}{Q_k} \tag{2.5}$$

with $Q_{A,r} - Q_{A,a}$ the net adhesion energy. The velocities of the colliding particles after collision are given as [1]

$$v_{1r,n} = v_{1i,n} - (1+e)\frac{C_m}{1+C_m} v_{i,n} \tag{2.6}$$

$$v_{2r,n} = v_{2i,n} + (1+e)\frac{1}{1+C_m} v_{i,n} \tag{2.7}$$

with $v_{i,n}$ the relative incident velocity of the two colliding particles. In figure 2.2 a frontal collision between two particles and the definition of the incident and rebound velocities are represented.

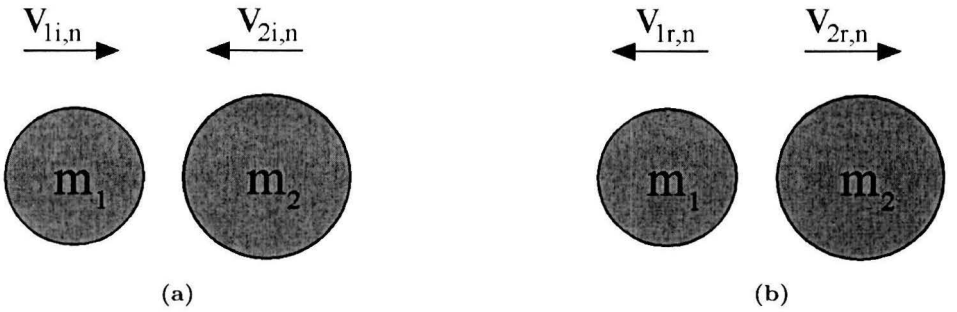

Figure 2.2: Frontal collision between two particles.
(a) Movement of the particles before the collision.
(b) Movement of the particles after the collision

The big advantage of this two-body approach is that the velocities of the two colliding particles are easy to determine when the coefficient of restitution is known. However the disadvantage of this method is that it is not possible to model removal of particles from a bed of particles. In the case of a proportionality factor that is equal to or smaller than one and an initial velocity of the second body equal to zero both bodies move in the same direction after the collision, which suggests that the incident particle penetrates the bed of particles.

2.2 Discrete element method

Another way to predict the outcome of a collision between an incident particle and a bed of particles is the discrete element method (DEM), which is based on Newton's second law of motion. In the DEM the particles are treated as discrete entities that interact with each other when they are in contact. In this method the collision is also divided in an approach phase and a restitution phase. The velocities and positions of the interacting particles are calculated by integration of Newton's second law of motion, which reads

$$\mathbf{F} = m\ddot{\mathbf{x}} \tag{2.8}$$

with $\mathbf{F}$ the sum of the forces working between the particles, $\ddot{\mathbf{x}}$ the acceleration vector of the particle and m is the mass of a particle. The acceleration $\ddot{\mathbf{x}}$ is assumed to be constant over a time interval Δt. The velocity at the end of the time interval can be calculated as

$$\dot{\mathbf{x}} = \dot{\mathbf{x}}_0 + \frac{\mathbf{F}}{m}\Delta t \tag{2.9}$$

with $\dot{\mathbf{x}}_0$ and $\dot{\mathbf{x}}$ the initial and final velocities of the particle. A second integration, using Euler's implicit scheme, leads to the particle displacement which reads

$$\mathbf{x} = \mathbf{x}_0 + \dot{\mathbf{x}}_0\Delta t + \frac{\mathbf{F}}{m}\Delta t^2 \tag{2.10}$$

with $\mathbf{x}_0$ and $\mathbf{x}$ the initial and final positions of the particle. The motion of the interacting particles is calculated by repeating the above procedure until the desired simulation time is reached. At the start of the calculation cycle (see figure 2.3) the initial positions and velocities are known and with these values the contact force between the interacting particles is calculated. With the calculated contact force the new acceleration, velocity and position of the particles is calculated. The interpenetration distance δ is determined with the new and old positions of the particles and is used for the calculation of the contact force at time t_n. This cycle continues until the desired simulation time t is reached.

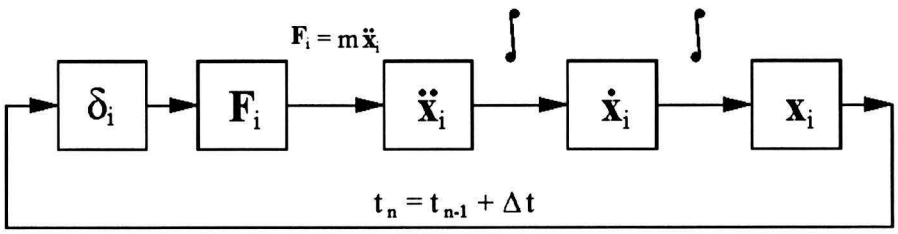

Figure 2.3: Calculation cycle of the discrete element method.

The force on the left hand side of equation 2.8 needs to be known to calculate the particle motion. The contact force between the interacting particles are described by the concepts of contact mechanics.

The numerical simulations presented in chapter 4 are made with a numerical code based on the model presented above. In chapter 4 the relations for the contact force are described for the two different phases of the collision.

The big advantage of this method is that the movement of all bed particles can be followed for the complete simulation time. By the use of contact mechanics the plastic deformation of the interacting particles are taken into account. A disadvantage of this method is that the time needed for a simulation is significantly longer than the time needed for the two-body approach.

2.3 Spring-damper model

In the spring damper model, as used by Tanaka et al. [11, 12], the particle motion of an incident particle colliding with a bed of particles is simulated with a discrete element method (DEM). In the DEM the particles interact with each other when they are in contact. When the particles are in contact with each other a contact force arises between the particles. The movement of the particles is described by the resultants of the force and moment of force exerted by the interacting particles. In the spring-damper model the force displacement relationship is approximated by a spring and a damper, as can be seen in figure 2.4.

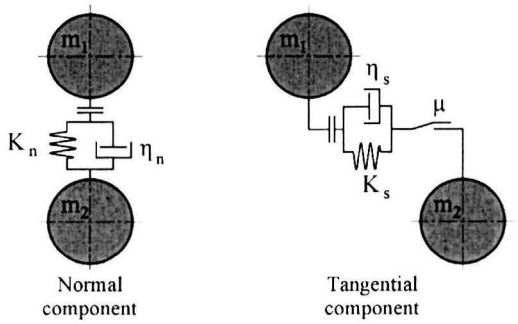

Figure 2.4: Spring-damper model for the force-displacement relationship.

The contact force between two particles is described by a spring and a damper. The friction between the interacting particles is described by a slider element. The disadvantage of this method is that the resulting coefficient of restitution is found to be constant and thus independent of the particle velocities [14]. The approximation of the contact force is given by the following differential equation

$$m\ddot{\mathbf{x}} + \eta\dot{\mathbf{x}} + K\mathbf{x} = 0 \tag{2.11}$$

with K the spring coefficient and η the damping coefficient. The solution of this equation for the rebound velocity is given as

$$v_r = \dot{x}|_{t=\pi/q} = -v_i exp(\gamma\omega_0\pi/q) \tag{2.12}$$

And therefore the coefficient of restitution becomes

$$e = \frac{v_r}{v_i} = exp(-\gamma\omega_0\pi/q) \tag{2.13}$$

where γ, ω_0 and q are constants dependent on the spring coefficient K and damping coefficient η, and therefore the coefficient of restitution is not dependent on the particle velocities of the colliding particles. A derivation of the differential equation is given in appendix B.

In my opinion the best method to use for the simulation of the particle interaction is the discrete element method in which the contact force is described with the theory of contact mechanics. With this method the coefficient of restitution is not constant. It is also possible to calculate the motion of several particles, in contrast with the two body collision model.

Chapter 3

Experimental methods and results

In order to investigate the post-collision behavior of an incident particle that hits a bed of particles several impaction experiments were performed. Two different experimental set-ups were used for the impaction experiments, a 3D set-up and a 2D set-up. With the 3D set-up impaction experiments with bronze micron particles are performed. In these experiments the post collision behavior of the bed particles and the incident particle are investigated with varying incident velocities and incident particle diameters [3]. In order to see the bed particle movement in more detail a 2D set-up was built in which bigger particles can be used for impaction experiments. In this chapter the two used experimental set-ups and the outcome of the experiments conducted on these set-ups, are presented.

3.1 '3D' experiments with micron particles

3.1.1 Experimental set-up

An experimental 3D set-up was designed and built to validate the two-body approach for the sticking model developed by van Beek [4] and will be used for performing impacting experiments on a powdery or a sintered surface. The particles used in this set-up can have a diameter that varies from 10 to 100 micron.

In figure 3.1.a a sketch of the experimental 3D set-up is presented. This experimental set-up consists of a column mounted on a chamber in which the pressure can be regulated from deep vacuum to an overpressure of several bars. By varying the height of the column and the pressure in the chamber the impacting speed of the incident particle can be adjusted. The incident particles are released from a particle feeder that is mounted in the top of the column. The particle feeder is a small reservoir were the incident particles are stored. These particles are released with an electrical triggering system that consists of an electromagnet and a steel ball. By dropping the steel ball on the particles in the reservoir some particles are forced out of the reservoir via a small hole. These particles fall on the bed of particles. This bed is situated on the object table that is mounted in the chamber. The impact angle of the incident particle can be adjusted by rotating the object table.

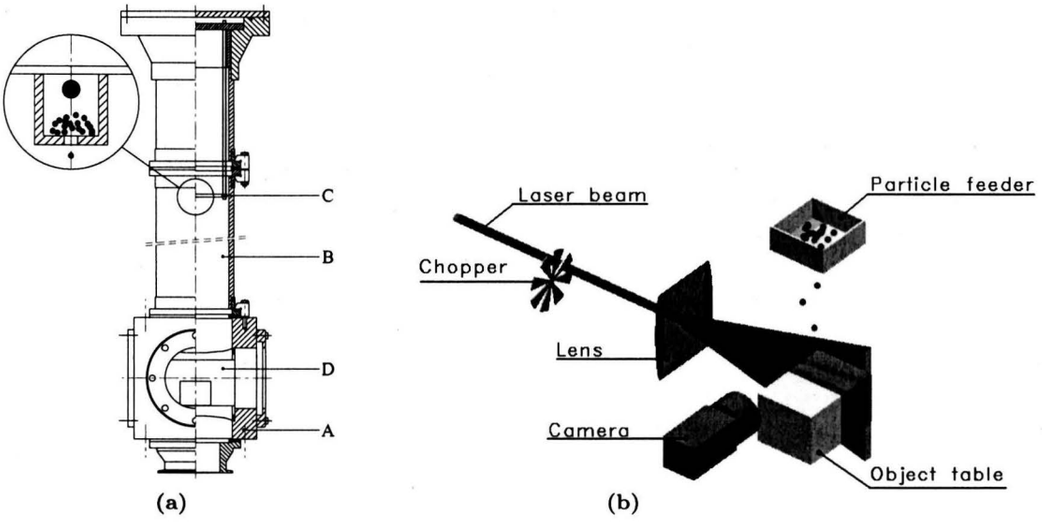

Figure 3.1: (a) Composition of the experimental 3D set-up;
A chamber, B column, C particle feeder and D object table.
(b)Schematic overview of the camera system.

In order to record the impact of the incident particle the chamber is optically accessible by two windows. The impact of the incident particle on the bed of particles is digitally recorded by a camera system. The camera used (JAI CV-M10) has a frame rate of 30 Hz. The images taken with the camera have a maximum resolution of 512 x 512 pixels. A schematic overview of the camera system is represented in figure 3.1.b. To track the incident particle and the removed bed particles they have to be visible for a number of time intervals. This is done by directing a continuous argon-ion laser beam through an optical chopper. By directing the laser beam through the chopper a continuous pulsating laser beam is created. This pulsating laser beam is guided through a cylindrical lens and transforms the beam into a light sheet. The particles that travel through this light sheet are illuminated several times in one camera image. In figure 3.2 some typical recorded images are given.

Figure 3.2: Typical recorded images of the impaction experiments.
(a) Bouncing of the incident particle.
(b) Removal of bed particles.

In the recorded images the incident particle and the powdery bed layer can be distinguished. In picture 3.2.a the incident particle hits the powdery layer and bounces off this powdery layer. In picture 3.2.b the impact speed of the incident particle is higher and therefore bed particles are removed. The impact speed of the incident particle correlates with the distance between two successive illuminations (blobs). The impact speed of the incident particle is calculated from:

$$v_i = f_{ch}\frac{h}{c} \tag{3.1}$$

with f_{ch} the frequency of the optical chopper, h the distance between two blobs (figure 3.3.b) and c the number of pixels per millimetre taken from a calibration image. The calibration image is represented in figure 3.3.a. The quantities c and h are measured manually with the software package Imagetool [19].

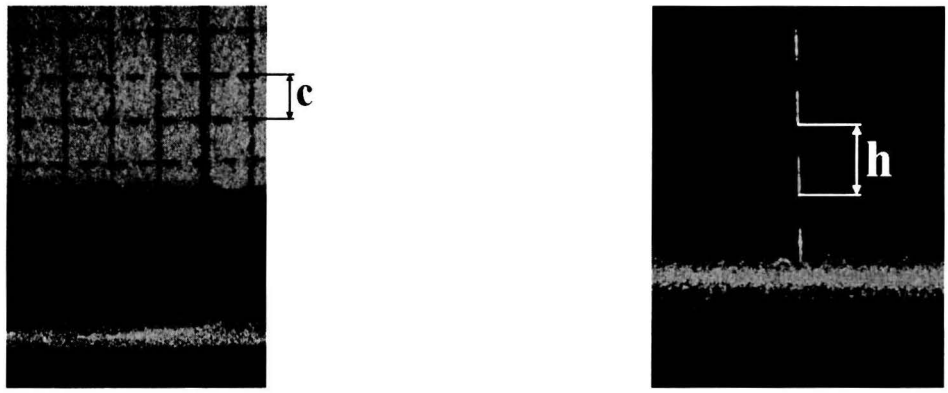

Figure 3.3: (a) Calibration image with a indicated grid of 1 x 1 mm for the determination of c. (b) The distance h between two blobs.

The impact speed of the incident particle can be adjusted by regulating the pressure inside the experimental set-up as stated before. But the impact speed of the particle is not only dependent on this pressure, it is also dependent on the particle size. All falling objects accelerate to their terminal velocity. At the terminal velocity of the falling object the gravitational force becomes equal to the friction force and the acceleration becomes zero. The terminal velocity of an object is mass dependent and therefore bigger particles shall reach a higher velocity under the same conditions as smaller particles. By increasing the pressure inside the experimental set-up the friction on the falling particle will increase and therefore the terminal velocity of the particle will decrease.

3.1.2 Used particles

The particles used for the impaction experiments are spherical bronze particles [16]. By sieving these particles with control sieves three batches with various diameter ranges are obtained. The particles of batch one have a diameter range of 71 to 75 micrometer, batch two has a diameter range of 50 to 53 micrometer and batch three a range of 25 to 32 micrometer. In figure 3.4 the three batches of bronze particles are shown.

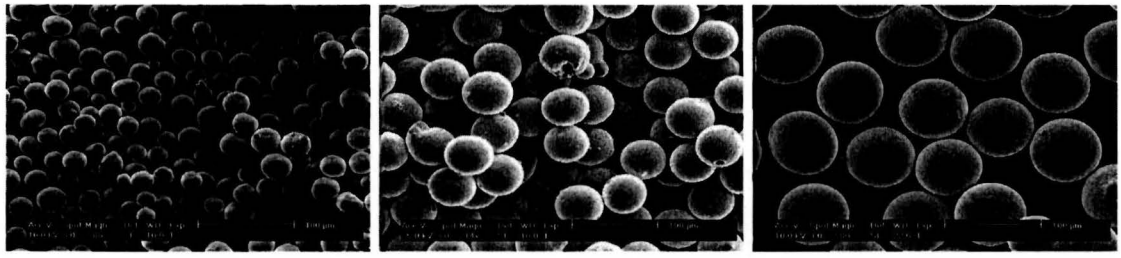

(a) (b) (c)

Figure 3.4: Sieved bronze particles used in the experiments.
(a) Particles in the range 25-32 μm (batch 1).
(b) Particles in the range 50-53 μm (batch 2).
(c) Particles in the range 70-75 μm (batch 3).

The average diameter of the particles is determined from the particle size distribution. The machine used for determination of the average particle diameter is the Coulter LS100. In figure 3.5 the results of the particle size distribution are given. The particles from batch 1 have an average diameter of 29 micron with a standard deviation of 3.3 micron. The average diameter of the particles from batch 2 have an average diameter of 52 micron and a standard deviation of 4.7 micron. The particles from batch 3 have an average diameter of 75 micron with a standard deviation of 4.6 micron.

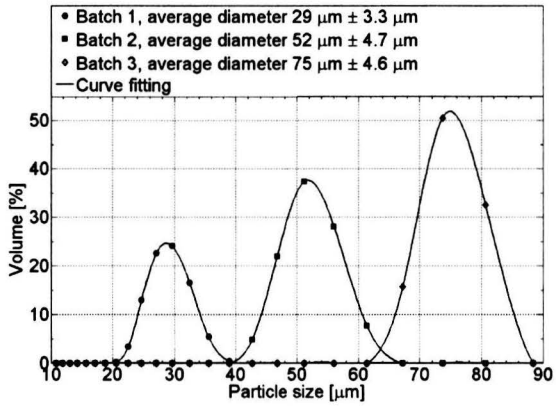

Figure 3.5: Results of the particle size distribution with the Coulter LS100.

The particles form batch 1 are used for the powdery bed and the particles from batch 1,2 and 3 are used as incident particles. The material properties of the bronze particles are given in appendix C.

3.1.3 Impaction on a powdery layer

With the bronze micron particles three different impacting experiments on a powdery bed were performed[1], in which the incident particle hits the bed under an angle of ninety degrees. In all the experiments the bed consisted of particles from batch one. The incident particles that were used for the experiments came from batch one for the first set of experiments, from batch two for the second set and from batch three for the last set of experiments.

In the experiments the post-collision behavior of the particles was examined with varying impact velocities. Depending on the impact speed of the incident particle three phenomena can be distinguished: the incident particle sticks to the bed of particles, the incident particle bounces of the bed or the incident particle removes particles out the bed of particles. In figure 3.6 recorded pictures of these phenomena are shown.

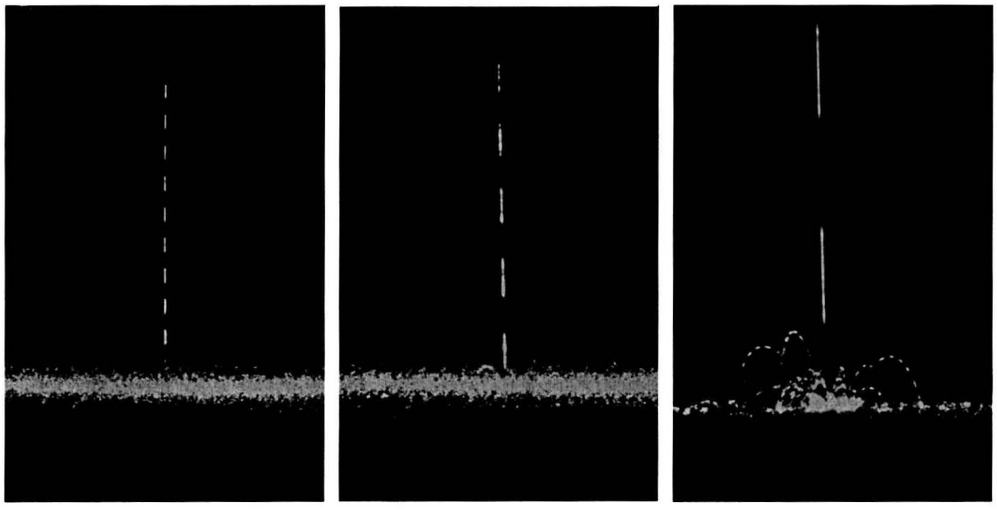

(a) (b) (c)

Figure 3.6: Post-collision behavior of an incident particle with an average diameter of 75 μm on a bed of particles with an average diameter of 29 μm.
(a) Sticking of the incident particle at an incident velocity of 0.16 m/s.
(b) Bouncing of the incident particle at an incident velocity of 0.41 m/s.
(c) Removal of bed particles at an incident velocity of 1.10 m/s.

The first set of experiments with an incident particle of 75 μm show that there are regimes in the velocity at which the different phenomena occur. The velocities found for sticking, bouncing and removal are given in figure 3.7.a, b and c. Sticking of the incident particle to the bed of particles can occur when the impact speed is 0.34 m/s or less. When the impact speed lies between 0.25 and 0.91 m/s the incident particle can bounce of the bed without removing other particles from the bed. When the incident speed is 0.33 m/s or higher removal of bed particles occurs, the amount of particles that are removed from the bed increase with increasing impact speed. The velocity regimes in which one of the phenomena occur show an overlap, as can be seen in figure 3.7.d.

[1]The results of these experiments are presented at the 13th International Heat Transfer Conference [3].

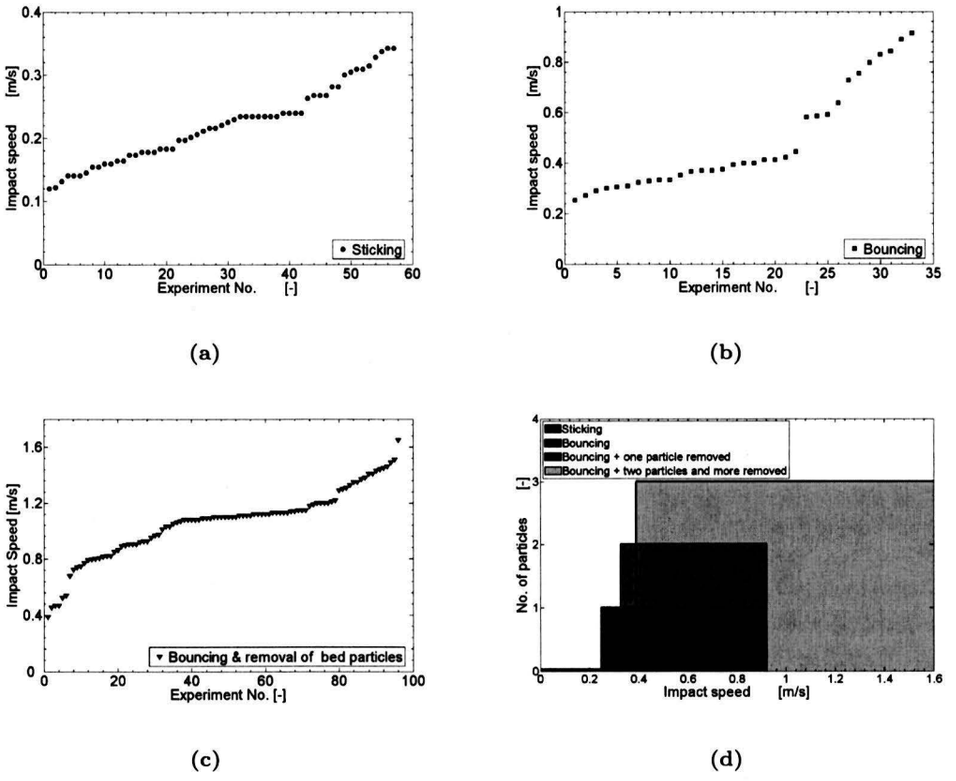

Figure 3.7: Post-collision behavior of an incident particle (d = 75 μm) as a function of the vertical impact speed.
(a) Sticking of the incident particle. (b) Bouncing of the incident particle.
(c) Removal of bed particles. (d) Overview of the velocity regimes.

As stated before there is an overlap in the velocity regime at which the different phenomena occur. So for a certain range in the impact speed, the post-collision behavior of an incident particle does not give the same outcome in repeated experiments. This overlap in velocity regimes can be ascribed to several things. First of all there is the variation in diameter of the bed particles, and therefore the bed is not homogenous and the top surface is not smooth. There is also a variation in the diameter of the incident particle. The outcome of the collision is also dependent of the place where the incident particle hits the bed particle; it can hit a bed particle exactly on the top or it can even hit several bed particles at the same time.

For the experiments with an incident particle with an average diameter of 52 μm respectively 29 μm also an overlap in velocity regimes occur, as can be seen in figure 3.8.a and 3.8.b. Sticking of the incident particle with an average diameter of 52 μm can occur when the impact speed is 0.58 m/s or less. Bouncing of the incident particle can occur when the impact speed lies between 0.44 and 0.96 m/s. Removal of bed particles occurs when the impact speed is 0.53 m/s or higher.

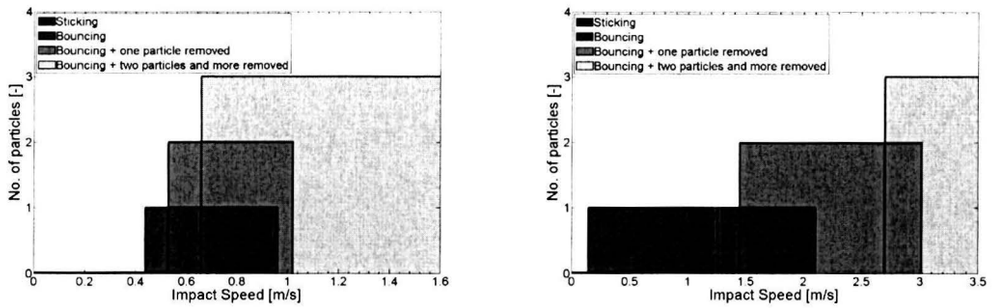

(a) (b)

Figure 3.8: Velocity regimes of the post-collision behavior.
(a) Incident particle diameter of 52 μm.
(b) Incident particle diameter of 29 μm.

When the incident particle has an average diameter of 29 μm sticking of the incident particle to the bed can occur when the impact speed is 0.41 m/s or less. If the impact speed lies between 0.15 and 2.1 m/s the incident particle bounces of the bed. Removal of bed particles start to occur when the impact speed is 1.45 m/s or higher. The data of the experiments with an incident particle of 52 μm respectively 29 μm is represented in appendix D.

In the experiments with an average incident particle diameter of 52 μm respectively 75 μm a distinction between the incident particle and the bed particles could be made due to the thickness of the streaks. In most cases of removal penetration of the incident particle in the bed did not take place. The experiments also show that increasing incident particle diameter results in a lower incident velocity at which removal of bed particles take place. That can be expected because the kinetic energy of the incident particle is a function of the mass and the velocity of the particle, with the same incident velocity the kinetic energy of a bigger particle will be higher. The kinetic energy at which removal of bed particles takes place is given in table 3.1.

Table 3.1: Kinetic energy at which removal takes place found in the experiments.

Diameter incident particle (μm)	Impact speed (m/s)	Kinetic energy ($*10^{-10} J$)
29	1.45	1.2028
52	0.53	0.9265
75	0.33	1.2595

3.1.4 Impaction on a sintered layer

For the experiment on a sintered bed, bronze particles with an average diameter of 52 μm were sintered in a nitrogen oven. The sintering took place in a nitrogen oven to prevent oxidation of the particles. The bronze particles were placed in the oven at room temperature and this temperature was maintained for 20 to 30 minutes. In this period of time the air in the oven is rinsed out with nitrogen to prevent oxidation of the sample. After this period of time the oven is started and the temperature is gradually raised to 500 °C in a period of 1 hour. If the oven temperature has reached 500 °C the oven stops heating and starts to cool down to room temperature in a period of 1 hour. The temperature profile of the oven is given in figure 3.9.

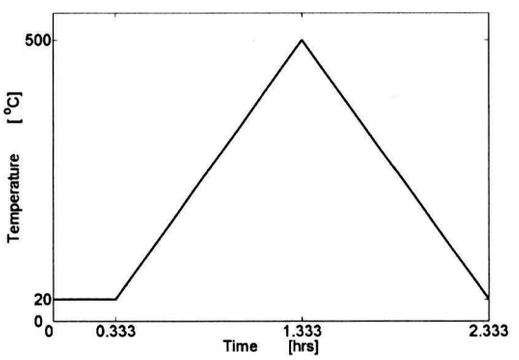

Figure 3.9: Temperature profile used for sintering inside a nitrogen oven.

The sintering grade of the bed is dependent of the X/D value [5], in which X is the neck diameter and D the diameter of the sintered particle. The neck diameter of the sintered particles is determined by measuring the neck diameter in a scanning electron microscoop (SEM), in figure 3.10 some pictures of the neck diameter measurement are given.

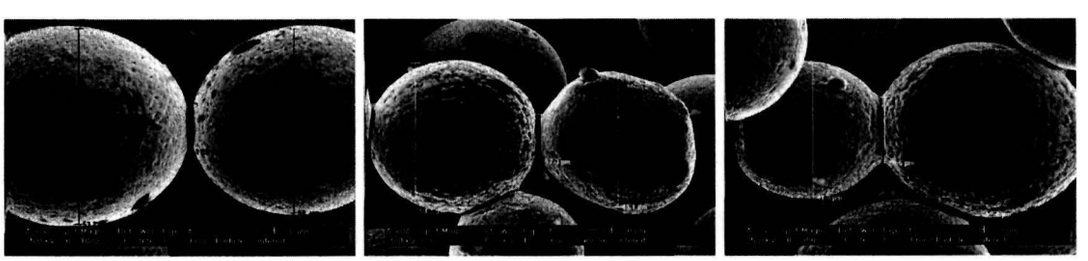

Figure 3.10: Pictures taken with the ESEM to determine the neck diameter.

In total 19 pictures of the sintered bed have been made. The average neck diameter for the sintered bed is then 13 μm. The X/D value becomes 0.24.

On the sintered bed impacting experiments were conducted with incident particles that had the same diameter as the bed particles, the results of these experiments are given in figure 3.11.

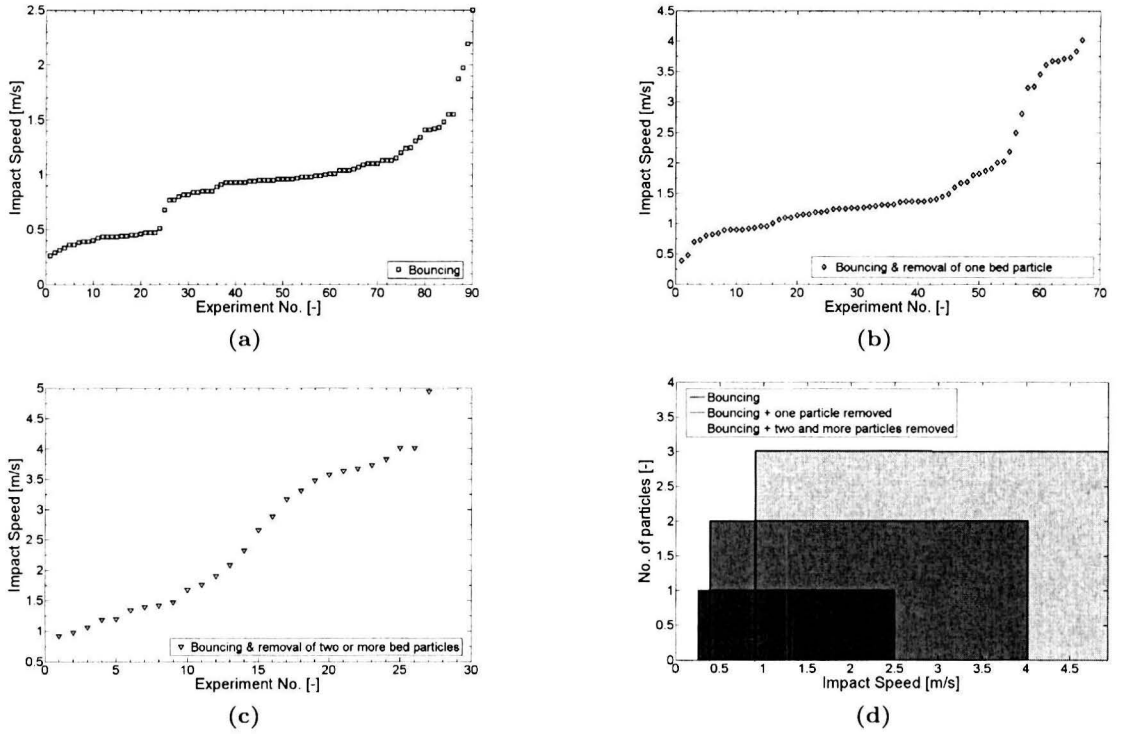

Figure 3.11: Post-collision behavior of an incident particle (d = 52 μm) hitting a sintered bed as a function of the vertical impact speed.
(a) Bouncing of the incident particle.
(b) Bouncing of the incident particle and removal of one bed particle.
(c) Bouncing of the incident particle and removal of two or more bed particles.
(d) Overview of the velocity regimes.

Also in these experiments an overlap in the velocity regimes are found. It can be seen from the experiments that if the impact speed of the incident particle lies between 0.26 m/s and 2.50 m/s (figure 3.11d) the particle can bounce of the bed without removing any bed particles. If the impact speed of the incident particle lies between 0.39 m/s and 4.02 m/s a particle bounces of the bed and removes a particle from the bed. Two or more particles are removed from the bed when the impact speed is 0.91 m/s or higher. The minimum impact velocity for removal of a particle out of the sintered bed is 0.39 m/s.

It was found that after impaction of incident particles on the sintered sample a hole was present in the sample. It seems that only the top layer of the sample was sintered and that underneath this sintered top layer a powdery layer was present. The velocity found at which removal starts to take place is in the same order as found by Abd-Elhady [1] for impaction on a powdery layer with a particle diameter of 54 μm. Abd-Elhady also performed impaction experiments on a sintered layer with a particle diameter of 54 μm and a X/D value of 0.22. In that experiment a velocity of 3.5 m/s was found at which removal starts to take place. In the experiment on a sintered sample with a X/D of 0.24 removal of one or two bed particles at a speed of 3.5 m/s was also found. It seems that the sample was indeed partially sintered and that there was also a powdery part present in the sample.

3.2 '2D' experiments with millimetre particles

3.2.1 Experimental set-up

In order to get a better insight on the dynamics of the bed particles after impact of an incident particle, a 2D set-up is designed and built that can house particles with a diameter in the order of millimetres. In figure 3.12.a a schematic overview of the 2D set-up is represented. The 2D set-up consists of a thin perspex container that houses the bed particles and a shooting mechanism to shoot the incident particle on the bed of particles. The perspex container is equipped with a movable back wall. Spacers are used to adjust the depth of the container to the diameter of the particles in the set-up. The distance between the front and the back wall of the container should be a little bigger than the diameter of the particles, to make sure that the particles can freely move after impact. The incident particle is shot on the bed particles with a shooting mechanism. This mechanism consists of a control valve (3 way valve) and a nozzle (see figure 3.12.b). The control valve is connected with a compressed air connection and a vacuum connection. When the control valve is connected with the vacuum connection, the incident particle sticks to the nozzle due to a pressure difference over the particle. When the control valve is switched to the compressed air connection the compressed air travels through the nozzle and the incident particle is shot to the bed particles. When the particle leaves the nozzle an air jet will travel behind the particle. To reduce the amount of air that travels behind the particle the control valve has to close immediately after the release of the particle. The time in which the nozzle is connected with the compressed air connection is controlled with an electronic circuit. The speed at which the particle leaves the nozzle is dependent on the pressure of the compressed air, by increasing the pressure a higher incident velocity is reached.

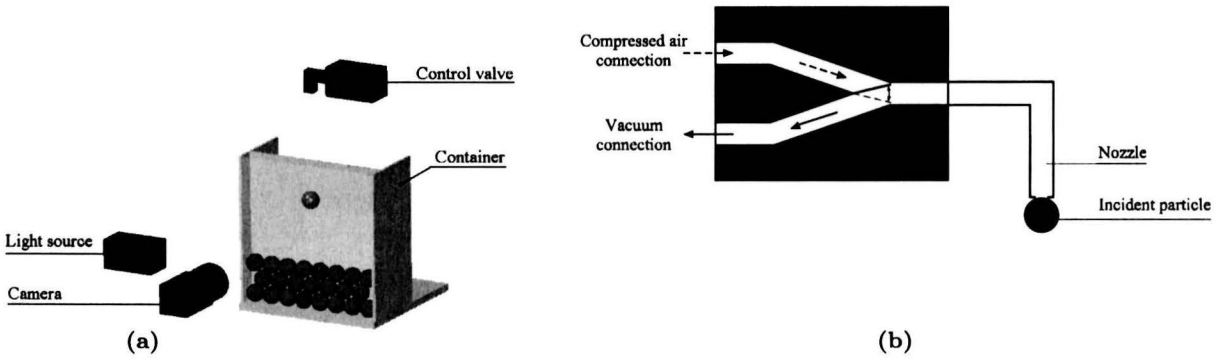

Figure 3.12: (a) Schematic representation of the experimental 2D set-up.
(b) Schematic representation of the shooting mechanism.

The impact of the incident particle with the bed particles is recorded with a high-speed camera (KODAK EKTAPRO HS Motion Analyzer 4540), with a record rate of 30 to 4500 full frames per second. The camera is positioned in front of the perspex container. The lighting of the set-up is obtained via a strong light source that comes from the side of the set-up, in order to prevent scattering of the light in the camera. In figure 3.13 some typical recorded images are represented.

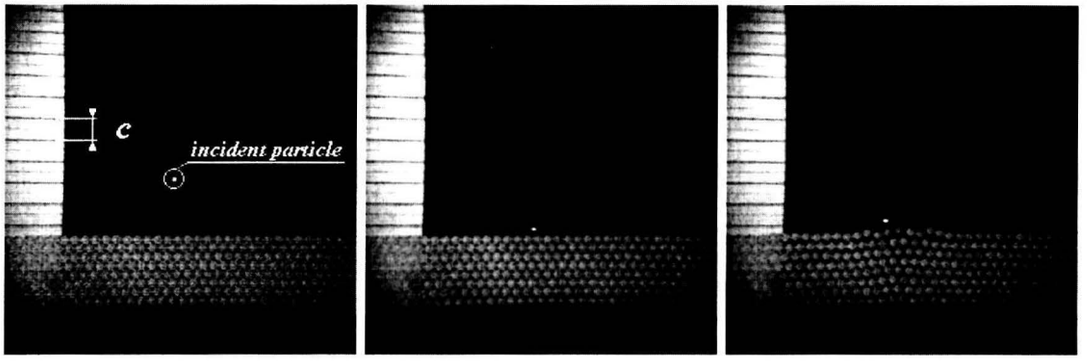

Figure 3.13: Typical recorded images of the impaction experiments.

In the recorded pictures the incident particle and the bed particles are easy to distinguish, the bed particles are more blurred than the incident particle. From the recorded image the speed of the incident particle can be determined via

$$v_i = \frac{h}{c\Delta t} \tag{3.2}$$

With h the traveled distance between two successive pictures and Δt the time between two successive pictures.

3.2.2 Used particles

The particles used for the impaction experiments on a 2D bed were polyhexamethylene adipamide (nylon) [17] and steel particles. The nylon particles have an average diameter of 5 mm and the steel particles have an diameter of 5 and 20 mm respectively. In order to investigate the bed dynamics at impact speeds varying from 1 to 10 m/s bed particles with a low mass are preferred, therefore nylon bed particles are used. Due to the low mass of the nylon particles less energy is needed to remove particles from the bed. The incident particle is made out of steel because a steel particle has a higher kinetic energy content as a nylon particle that is moving at the same velocity. In order to measure to contact time between the incident particle and a target particle heavier particles are needed. Therefore steel particles of 20 mm were used as bed and incident particle. The material properties of the used particles are given in appendix C.

3.2.3 Impaction on a nylon bed

Impacting experiments on a bed of nylon particles are performed with several impact speeds. The bed is stacked in such a way that the uneven layer has 42 particles and the even layer 41 particles. The impact speed of the incident particle is varied between 1.5 and 8 m/s. In figure 3.15 the results of an impact with a speed of 4.5 m/s are represented, these results are also included as a movie on the additional cd-rom (Figure-315.wmv). The experiments are recorded with a frame rate of 250 frames per second which results in a time step of 4 milliseconds between two successive frames.

When the incident particle hits the bed of particles a force transfer travels through the bed of particles and particles nearby the the point of impact start to move upward in a triangular shape (region 1). At the base of this triangular shape a second triangular shape (region 2), that points downwards, arises as can be seen in figure 3.14. There is also movement of particles in the upper three layers of the bed along side the point of impact. Besides that there are two regions (region 3) in which there is no noticeable movent of the bed particles. The target particle is hit slightly to the right of the center by the incident particle. Therefore the incident particle travels to right. It can be seen that the particles at the left side of the impact point travel a bit higher than the particles on the right side (figure 3.15).

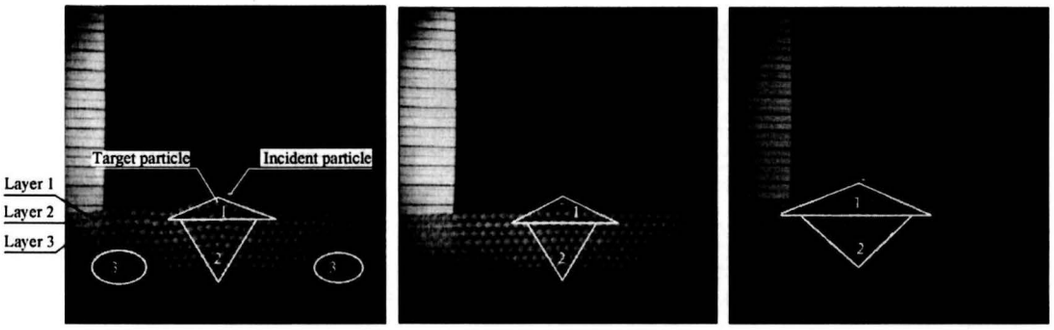

Figure 3.14: Representation of the regions in which particle movement takes place at different incident velocities.
(a) Regions at an incident velocity of 4.5 m/s 8 ms after impact.
(b) Regions at an incident velocity of 2.6 m/s 8 ms after impact.
(c) Regions at an incident velocity of 7.5 m/s 8 ms after impact.

The particles in the first region are the particles to which most of the energy is transferred and therefore they have the biggest upward motion. From all the particles in region 1 the target particle is the particle that undergoes the largest displacement of all bed particles. The particles at the bottom of region 2 and the particles in layer three and two are the first particles that start falling down. They start to fall down approximately 28 milliseconds after impact of the incident particle. After 40 milliseconds the particles in the first layer and the particles in the top of region 2 start to fall down again. The particles in the first layer start to move down after 64 milliseconds and the target particle and its two neighbors after 80 milliseconds.

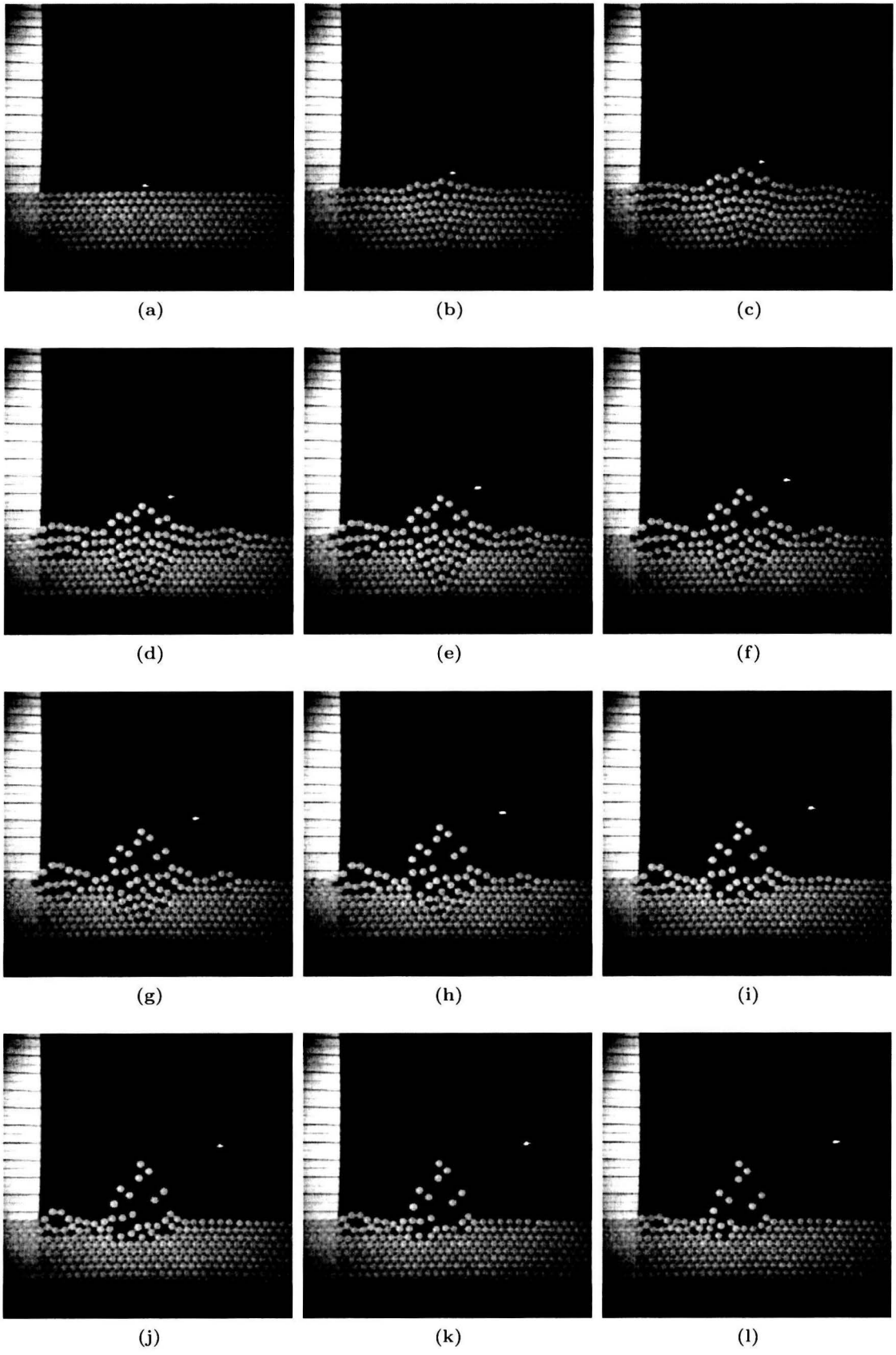

Figure 3.15: Collision of a steel particle on a nylon bed of particles with an impact speed of 4.5 m/s. Time step between two successive pictures is 8 ms.

The amount of particles that move upward and the distance they move upward are dependent on the incident velocity. In figure 3.14.b and 3.14.c the result is given for an impact with an incident velocity of 2.6 m/s and 7.5 m/s at 8 milliseconds after impact. In appendix E, and on the additional cd-rom (Figure-E1.wmv and Figure-E2.wmv), the complete results are given for a time span of 88 milliseconds with a time step of 8 milliseconds. It can be seen that when the incident velocity decreases the amount of particles that move upward decreases, as well as the particles in region 1 and 2 but also the particles in the upper layers. The height of the upward moving particles also decreases with decreasing velocity. The region in which there is now particle movement visible becomes larger. With increasing incident velocity the amount and the height of the upward moving particles increases, and the region in which no particle movement takes place decreases. The particle motion after collision corresponds with the results found by Tanaka [12], as can be seen in appendix F.

Influence of impact position

With the experiments the influence of the impact position on the velocity ratio is investigated. The incident and rebound velocity of the incident particle is determined for three different impact positions. In figure 3.16 a schematic representation of the impact positions is given. The first impact position (case 1) is where the incident particle strikes the target particle in the middle, which results in a local impact angle α of 90 degrees. The impact angle α is defined as the angle between the center line of the colliding particles and the horizontal. In case 2 the incident particle strikes between two bed particles and results in an impact angle of 60 degrees. In case 3 the impact angle is 75 degrees.

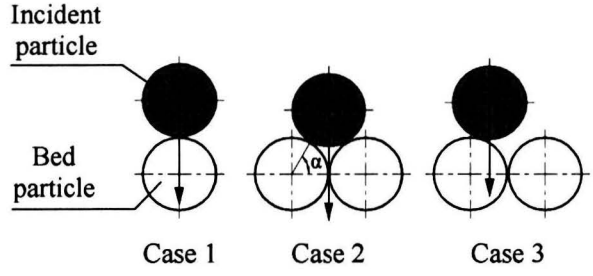

Figure 3.16: Definition of the impact position of the incident particle on the bed particle.

The incident velocity of the incident particle is varied between 1 and 8 m/s. In figure 3.17.a the rebound velocity of the incident particle is given as a function of the incident velocity. The velocity ratio of the incident particle is defined as the rebound velocity divided by the incident velocity, and is represented in figure 3.17.b.

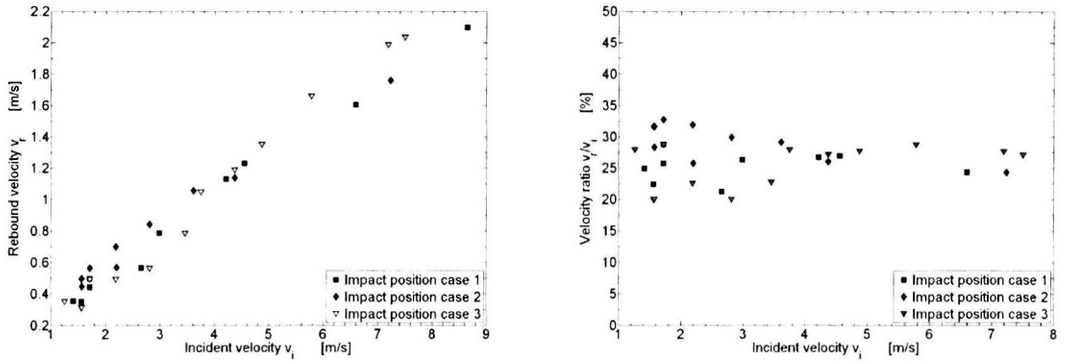

(a) (b)

Figure 3.17: (a) Rebound velocity as a function of the incident velocity.
(b) Velocity ratio as a function of the incident velocity.

It can be seen that an increase in the incident velocity leads to an increase in the rebound velocity of the incident particle. The velocity ratio lies between 22 and 30 percent, with some peaks to a higher and a lower value for the lowest incident velocities. In case 1, were the incident particle hits the target particle in the middle, the velocity ratio is 25 percent. For case 2 a velocity ratio of 30 percent is found. For case 3 the velocity ratio fluctuates between the velocity ratios for case 1 and 2. The fluctuation of the velocity ratio for case 3 is a consequence of the definition for the impact cases. The incident particle in case 3 can hit the target particle just off center and then the velocity ratio should be close to the value for the velocity ratio of case 1. When the incident particle hits almost two bed particles the velocity ratio should be close to the value of the velocity ratio of case 2.

Influence of the number of bed layers

With the experiments the influence of the number of bed layers on the velocity ratio of the incident particle is also investigated. In the experiments the height of the nylon bed is varied between 9, 7, 5 and 0 bed layers. The velocity ratios for the four different bed heights are presented in figure 3.18.a, b, c and d.

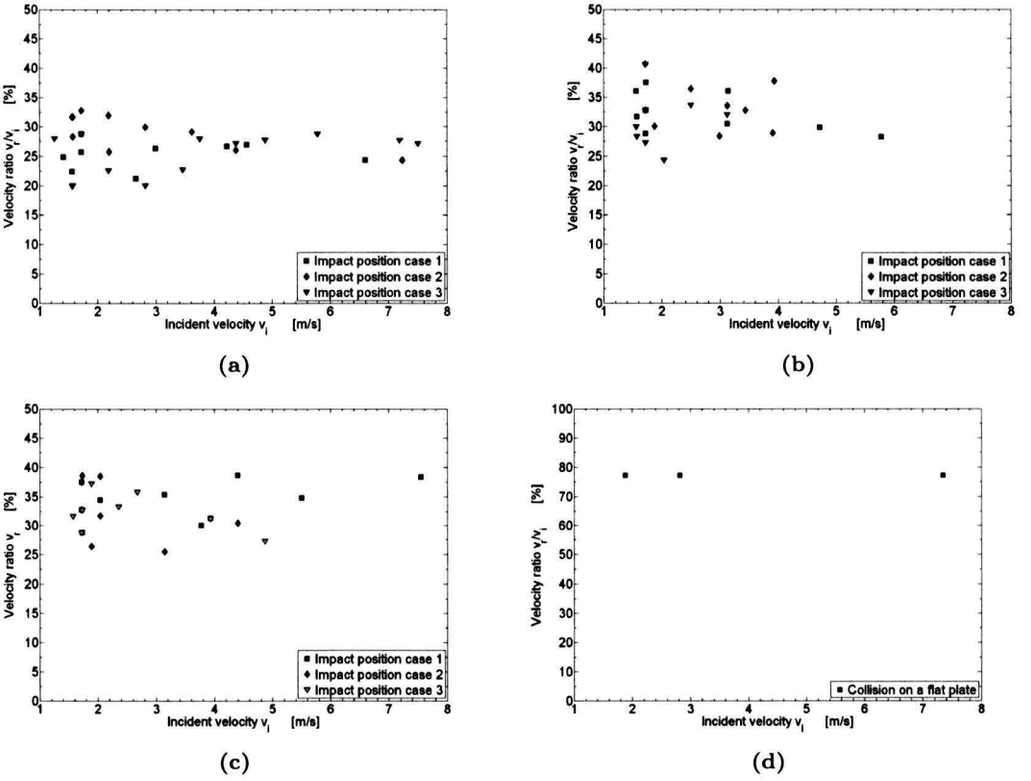

Figure 3.18: Velocity ratio as a function of the incident velocity for different bed heights.
(a) For 9 bed layers. (b) For 7 bed layers.
(c) For 5 bed layers. (d) For 0 bed layers.

It can be seen that with an increasing height of the bed the velocity ratio decreases. In the case of 9 bed layers the velocity ratio lies between 20 and For a bed height of 7 layers the velocity ratio lies between 26 and 35 percent. In the case of 5 layers the velocity ratio lies between 32 an 38 percent. In the case when the incident particle hits the bottom of the perspex container (0 bed layers) the velocity ratio is the highest and is approximately 80 percent.

In figure 3.19 the outcome of the collision with a steel ball on three different nylon beds is represented. The impact speed of the incident particle is 5.8 m/s and the time between two successive pictures is 8 ms. It can be seen that the areas in which the movement of the bed particles take place are dependent on the amount of layers. When the amount of bed layers decrease the area in which there is no particle movement becomes smaller.

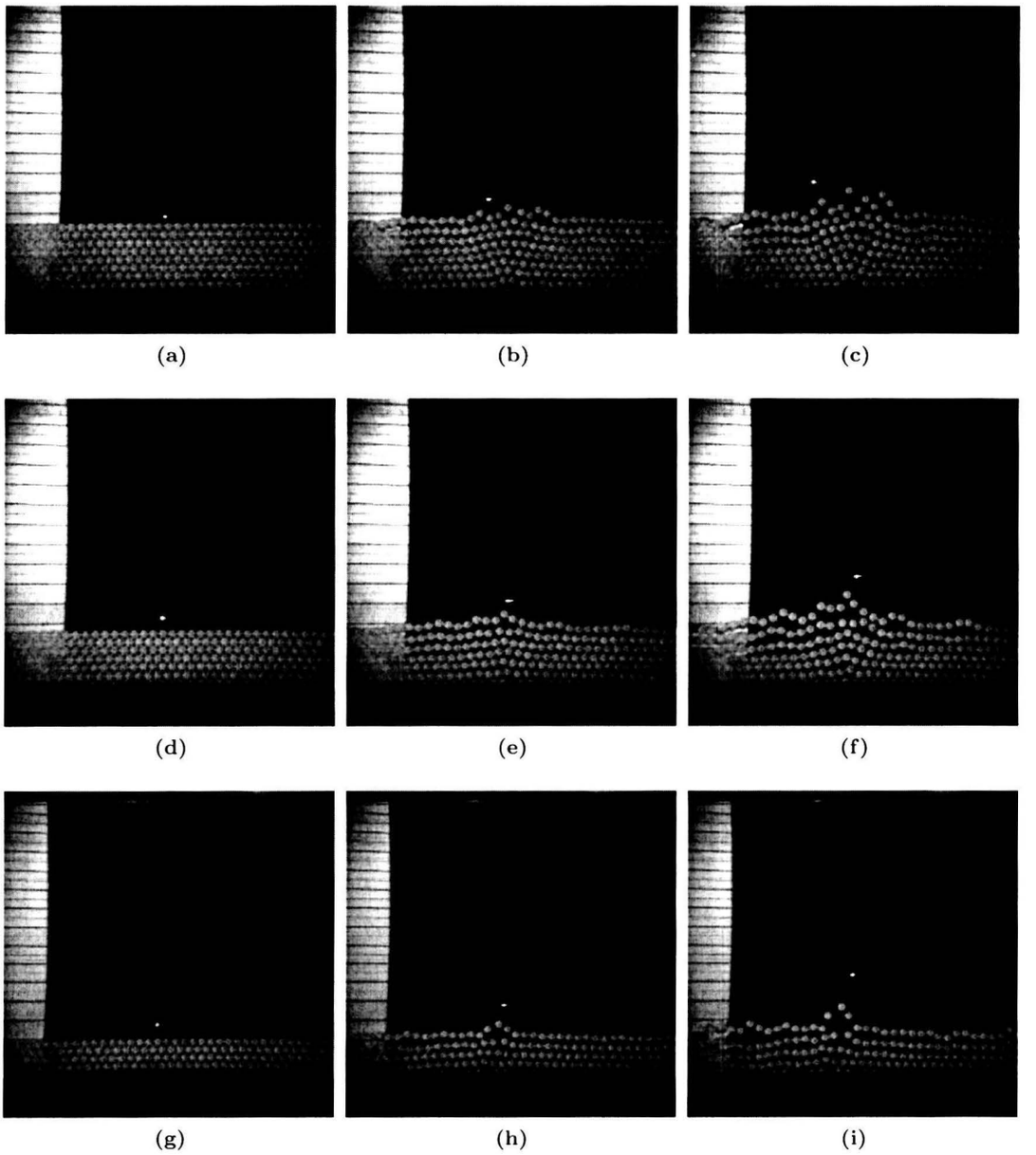

Figure 3.19: Collision of a steel particle on a nylon bed of particles with an impact speed of 5.8 m/s. Time step between two successive pictures is 8 ms.
(a-c) 9 bed layers.
(d-f) 7 bed layers.
(g-h) 5 bed layers.

Influence of the bottom

The influence of the bottom wall on the outcome of a collision between an incident particle and a bed of particles is investigated. The nylon bed of particles is situated on a layer of foam rubber. The rebound velocity as a function of the incident velocity is presented in figure 3.20.a the velocity ratio of the incident particle is presented in figure 3.20.b.

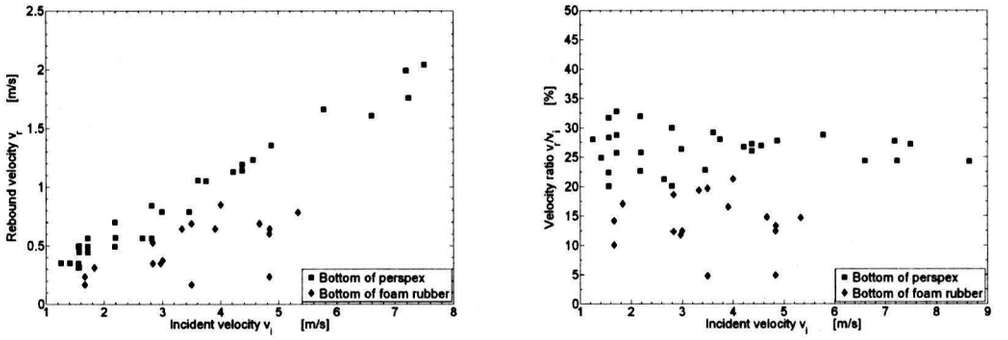

(a) (b)

Figure 3.20: (a) Rebound velocity as a function of the incident velocity.
(b) Velocity ratio as a function of the incident velocity.

It can be seen that in the case of the flexibele bottom the rebound velocity is much lower at the same incident speed in comparison with an non flexibele bottom (perspex), and therefore the velocity ratio is also lower. In figure 3.21 the outcome of a collision on a bed of nine layers on a foam rubber bottom is represented. The results are also included as a movie on the additional cd-rom (Figure-321.wmv). The impact speed of the target particle is 4.6 m/s and the time step between two successive pictures is 8 ms.

In comparison with figure 3.15 it can be seen that the movement of the bed particles is smaller. In area one and two there is hardly any movement of the bed particles noticeable. The movement of the particles in the upper layers is also smaller. In the case of a flexible bottom only movement of the particles near the impact point is visible. So most of the energy transferred from the incident particle to the bed particles is dissipated in the foam rubber on which the bed is situated. It can be concluded that the bottom wall on which the particles are situated plays an important role in the outcome of the collision.

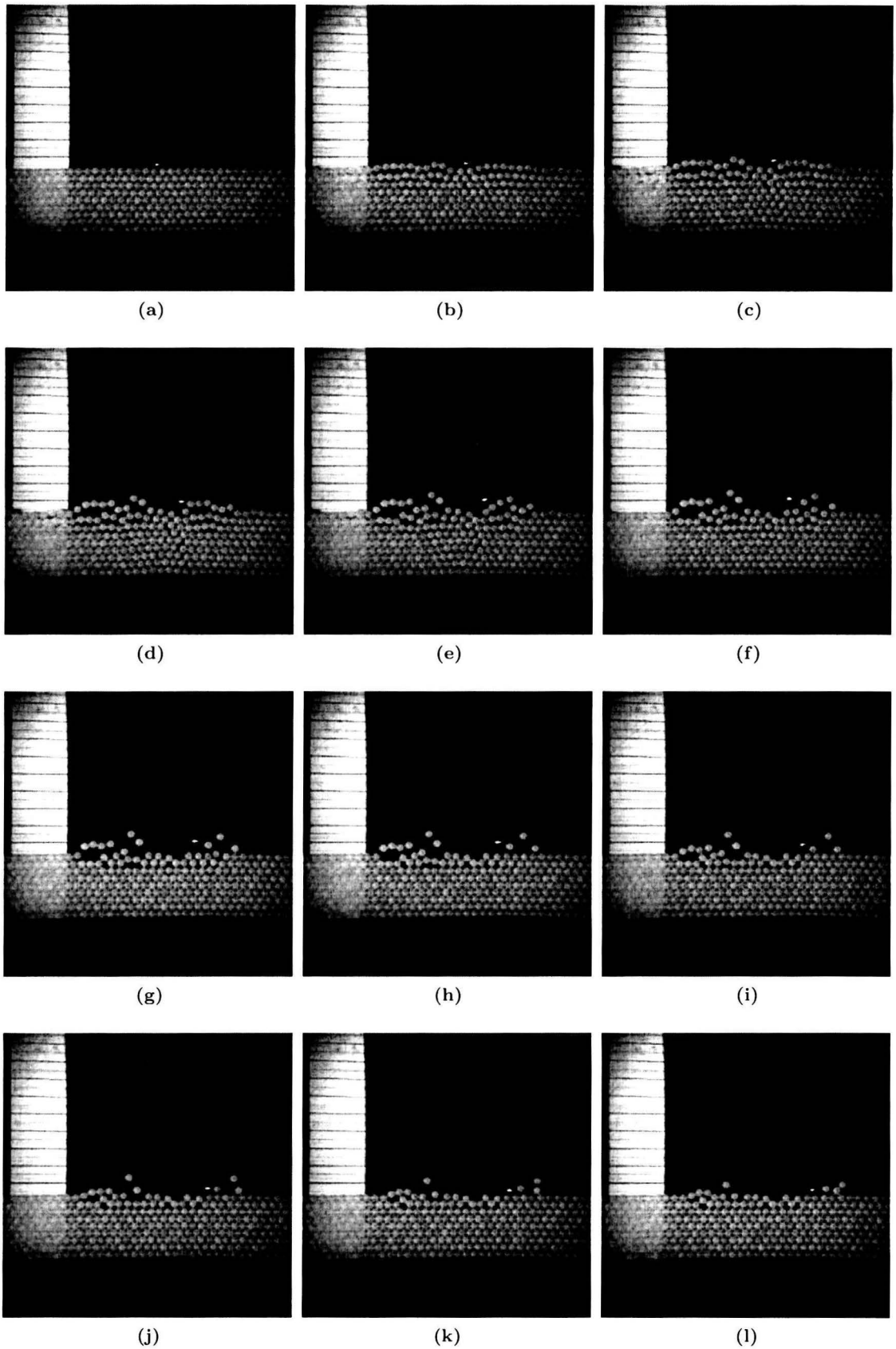

Figure 3.21: Collision of a steel particle on a nylon bed of particles with an impact speed of 4.6 m/s and a bottom of foam rubber. Time step between two successive pictures is 8 ms.

3.2.4 Impaction on a steel bed

The contact time of the incident particle with the target particle is also investigated with the 2D set-up. With the used camera system it was not possible to measure to contact time in the case of a steel incident particle colliding with a bed of nylon particles, both with a diameter of 5 mm. Therefore steel particles with a diameter of 20 mm were used. The bed consists of 15 steel particles and are stacked rectangular (5x3x1). The incident particle strikes the middle bed particle with an incident velocity of 2.7 m/s. The rebound velocity of the incident particle is 1.52 m/s. In order to measure to contact time a scanning rate of 47.000 frames per second is used, which results in a time step of 0.213e-4 seconds. In figure 3.22 the results of the collision are presented. The results are also included as a movie on the additional cd-rom (Figure-322.wmv). In figure 3.22.a the incident particle is still approaching the target particle and in figure 3.22.b the incident particle strikes the target particle with a velocity of 2.7 m/s. After impact the incident particle deforms and energy is transferred to the target particle (figure 3.22.c). The target particle starts to move downward 0.42e-4 seconds after impact (figure 3.22.d) and stops moving downward 0.255 milliseconds after impact (figure 3.22.n).

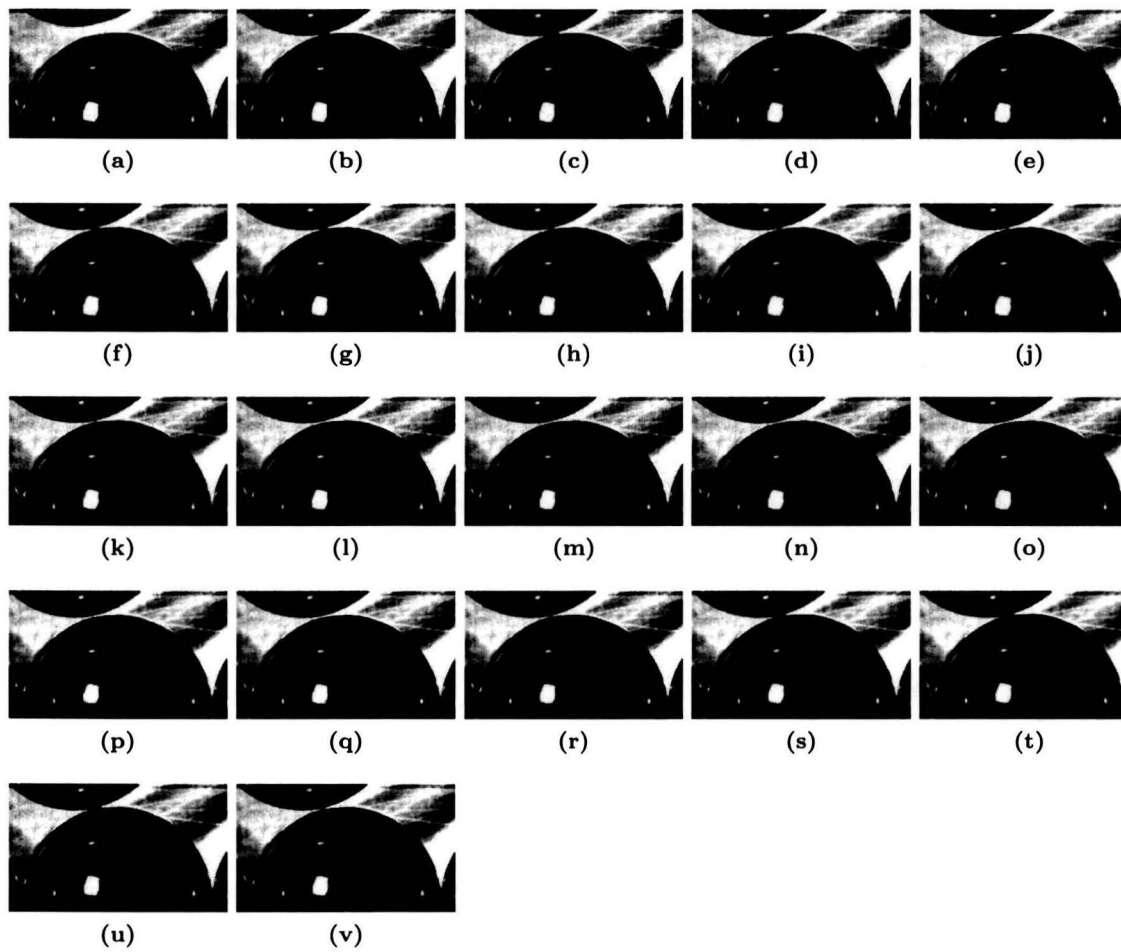

Figure 3.22: Collision between a steel incident particle and a rectangular bed of steel particles (5x3x1).

The target particle starts moving upward again 0.298 milliseconds after impact (figure 3.22.p) and hits the incident particle 0.383 milliseconds after impact (figure 3.22.s). The incident particle bounces off the target particle 0.404 milliseconds after impact (figure 3.22.u). So the contact time of the incident particle is 0.404 milliseconds.

3.3 Error analysis

The incident velocities of the incident particle are calculated from independent quantities as the chopper frequency, the distance between the blobs and the dimension of the camera image. All these quantities contain an experimental, random error and therefore lead to an error in the calculated velocity. In table 3.2 the random errors for the measured quantities are given, for a more detailed description of the error analysis the reader is referred to van Beek [4].

Table 3.2: Random errors made in the measured quantities.

Quantity	Symbol	Error
Chopper frequency	f_{ch}	0.5%
Distances	h,H and C	1 pixel

The uncertainty in velocity v, where v is a function of n variables x_k with a random absolute error u_k, can be written as

$$u_v = \sqrt{\sum_{k=1}^{n} \left(\frac{\partial v}{\partial x_k} u_k \right)^2} \tag{3.3}$$

The uncertainty in the measured velocity due to random errors can be derived using equation 3.3. The relative error in the measured velocity for a typical situation with the 3D and 2D set-up

	3D set-up	
v_i	= 0.1 ±0.007 m/s,	relative error 7% with
f_{ch}	= 300 ±1.5 Hz	
h	= 25 ±1 pixel	
c	= 64 ±1 pixel/mm	

	2D set-up	
v_i	= 1.5 ±0.1 m/s,	relative error 7% with
h	= 10 ±1 pixel	
c	= 160/10 ±1 pixel/cm	
Δt	= 0.004 ±0 sec	

The relative error made in the measured velocity of the incident particle is for both experimental set-ups 7 percent in the worst case scenario. The error made in the incident velocity decreases when the measured distance h increases, because the influence of 1 pixel on the measured distance reduces.

3.4 Conclusions

Impaction experiments were carried out in a 3D set-up in order to investigate the post-collision behavior of the incident particle and the bed particles. These experiments show that three different phenomena can occur during an impact of an incident particle on a bed of particles. The incident particle can stick to the bed or it can bounce off the bed. When the incident particle bounces off the bed, particles can be removed from the bed. The velocity at which removal occurs is found to be dependent on the diameter of the incident particle. With an increasing incident particle diameter, and a constant bed particle diameter, the removal velocity decreases. The velocities at which the post-collision phenomena take place show an overlap. This overlap in velocity regimes can be explained by several things. First of all the inhomogeneous bed due to the variation of the bed particle diameter. There is also an variation of the incident particle diameter.

Impaction experiments with the 2D set-up show that the velocity ratio of the incident particle is dependent on the impact position and the amount of bed layers. With a decreasing number of bed layers an increase in the velocity ratio is found. With a decreasing number of bed layers less particles are situated in the bed, so less energy is transferred to the bed particles. The outcome of the collision is also dependent on the bottom on which the particle bed is situated. With the experimental set-up it is also possible to measure the contact time between the colliding particles.

Chapter 4

Numerical method and results

In order to model the dynamics of colliding particles a model is needed that simulates this collision behavior. In this chapter the interaction between an incident particle and a bed of particles is simulated numerically with a code written by Abd-Elhady [1]. The numerical code is based on the discrete element method (DEM). The contact forces between the particles are described by contact mechanics. In this chapter the results of a collision between a steel particle and a orthorhombic bed of nylon particles are described. In this simulation the particle movement of the bed particles after collision is investigated and the velocity ratio of the incident particle is determined for different incident velocities. The contact time of a steel particle colliding with a rectangular bed of steel particles is also determined. The results are compared with the results of the experiments.

4.1 Numerical model

The numerical model used for the simulation of the interaction between a colliding particle and a bed of particles is based on the discrete element method (DEM). The movement of the particles is calculated via Newton's second law of motion, which has the form

$$\mathbf{F} = m\ddot{\mathbf{x}} \tag{4.1}$$

The velocity of the particles is determined by integrating equation 4.1 and reads

$$\dot{\mathbf{x}} = \dot{\mathbf{x}}_0 + \frac{\mathbf{F}}{m}\Delta t \tag{4.2}$$

A second integration leads to the particle displacement which reads

$$\mathbf{x} = \mathbf{x}_0 + \dot{\mathbf{x}}_0\Delta t + \frac{\mathbf{F}}{m}\Delta t^2 \tag{4.3}$$

To follow the motion of the interacting particles the procedure is repeated several time-steps until for all interacting particles the desired simulation time is reached.

The numerical code is written by Abd-Elhady [1] and Abd-Elhady et al [2] using the numerical package C++ and the Euler's implicit scheme for numerical integration. The Euler implicit scheme is used because of its stability and accuracy at large integration time-steps. To solve equation 4.1 the left hand-side needs to be known. The contact forces between colliding particles are based on the theory of contact mechanics, and are briefly described in the next section.

The accuracy of the solution is strongly dependent on the integration time-step Δt. In the simulations the time step is taken several orders smaller as the time in which two colliding particles are in contact with each other, the contact time. The contact time, for a purely elastic collision, is given as [6]

$$\tau = 2.94 \left(\frac{m^2}{k_c^2 v_{i,n}} \right)^{\frac{1}{5}} \tag{4.4}$$

where $v_{i,n}$ is the relative normal incident velocity and the coefficient k_c is defined as

$$k_c = \frac{16}{15} E^* R^{*\frac{1}{2}} \tag{4.5}$$

with R^* and E^* defined as

$$R^* = \frac{R_1 R_2}{R_1 + R_2} \tag{4.6}$$

$$E^* = \left(\frac{1 - \nu_1^2}{E_1} + \frac{1 - \nu_2^2}{E_2} \right)^{-1} \tag{4.7}$$

with R the radius of the colliding particles, ν the Poison ratio and E the Young's modulus of elasticity, with the subscripts 1 and 2 representing the interacting particles 1 and 2 respectively. In figure 4.1 the contact time is given for three cases of two colliding particles: a collision between a steel and a nylon particle, a collision between a two nylon particles and a collision between two steel particles. In the first two cases the diameter of the particles is 5 millimetre and in the last case the diameter is 20 millimetre. It can be seen that the contact time has a negative exponential curve. When the incident speed is zero the contact time is infinite and with increasing speed the contact time decreases. The contact time is in the order of 1e-5 seconds for all three different cases, which means that the time step in the numerical calculations should at least be one order smaller as 1e-5 seconds.

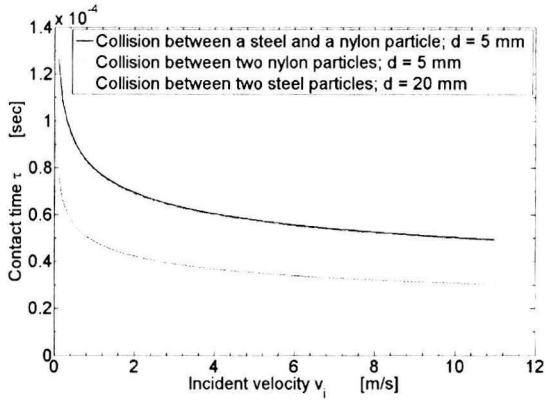

Figure 4.1: Contact time as a function of the incident velocity.

4.1.1 Contact forces between colliding particles

When particles collide a contact force develops between the colliding particles. This contact force can be divided in a normal contact force (F_{cn}) and a tangential contact force (F_{ct}). The normal contact force acts in the line of centers between the colliding particles and the tangential force acts perpendicular to the line of centers, as can be seen in figure 4.2.a.

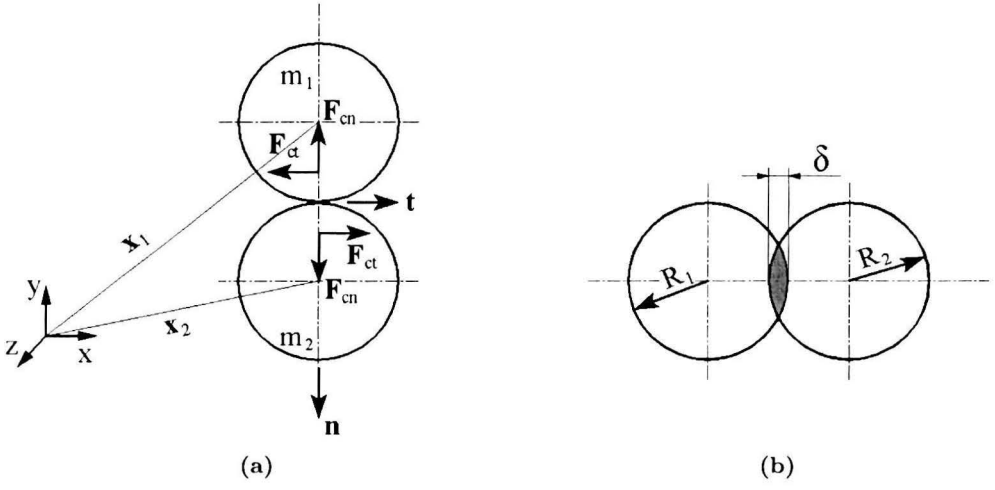

Figure 4.2: (a) Schematic representation of the contact forces between two colliding particles. (b) Schematic representation of the interpenetration distance δ between two colliding particles.

The contact force between colliding particles depends on the relative velocity and the phase of the collision. Two different phases can be distinguished in a particle collision, namely the approach phase and the restitution phase. During the approach phase a contact force between the colliding particles is built up until the relative normal velocity of the colliding particles becomes zero. In the approach phase deformation of the colliding particles takes place. When the stress between the colliding particles does not exceed the yield stress of the colliding particles only elastic deformation takes place. A pure elastic collision is limited by the elastic deformation limit δ_{el} [4] and is given as

$$\delta_{el} = \left(\frac{2}{3}\pi\right)^2 \frac{R^*}{\left(\frac{4}{3}E^*\right)^2} y^2 \tag{4.8}$$

with y the elastic load limit and is equal to 1.59 times the Yield stress σ_y. Plastic deformation of the colliding particles will take place when the stress between the colliding particles exceeds the yield stress. The normal contact force between colliding particles in the case of an elastic collision is described by the Hertz theory [9] as

$$\mathbf{F}_{cn} = |k\delta^{\frac{3}{2}}|\mathbf{n} \tag{4.9}$$

With δ the interpenetration distance between the interacting particles, as shown in figure 4.2.b, and is defined as

$$\delta = (R_2 + R_1) - |\mathbf{x}_2 - \mathbf{x}_1| \tag{4.10}$$

Where $\mathbf{x}$ is the position vector of the particle. The normal unit vector $\mathbf{n}$ is defined as

$$\mathbf{n} = \frac{\mathbf{x}_2 - \mathbf{x}_1}{|\mathbf{x}_2 - \mathbf{x}_1|} \tag{4.11}$$

Coefficient k is defined as

$$k = \frac{4}{3}E^* R^{*\frac{1}{2}} \tag{4.12}$$

When the interpenetration distance δ exceeds δ_{el} plastic deformation of the colliding particles starts. The normal contact force for an elastic-plastic collision is given by Thornton and Ning [13] as

$$\mathbf{F}_{cn} = |F_{el} + \pi y R^*(\delta - \delta_{el})|\mathbf{n} \tag{4.13}$$

where F_{el} is the average elastic force developed during a purely elastic collision just before the plastic deformation starts. The average elastic force is given as

$$F_{el} = k\delta_{el}^{\frac{3}{2}} \tag{4.14}$$

At the end of the approach phase, when the relative normal velocity is zero, the restitution phase starts. In the restitution phase the contact decreases from its maximum value to zero. The normal contact force during the restitution phase is given as [13]

$$\mathbf{F}_{cn} = \left| \frac{4}{3} E^* R_c^{\frac{1}{2}} (\delta - \delta_p)^{\frac{3}{2}} \right| \mathbf{n} \tag{4.15}$$

Where R_c is the contact radius between the two colliding particles and δ_p the remnant plastic deformation at the end of the approach phase. The remnant plastic deformation is calculated with equation 4.13 and 4.15: the contact force at the end of the approach phase (equation 4.13) should be equal to the contact force at the beginning of the restitution phase (equation 4.15). The contact radius R_c is equal to R^* in the case of an elastic collision and when the collision is plastic-elastic the contact radius reads

$$R_c = \frac{4E^*}{3F_{cn}} (R^* \delta)^{\frac{3}{2}} \tag{4.16}$$

The tangential contact force is related to the total force in normal direction via Coulomb's friction law. The total force in normal direction is given as

$$\mathbf{F} = \mathbf{F}_{cn} + \mathbf{F}_{adh} \tag{4.17}$$

with $\mathbf{F}_{adh}$ the adhesion force that appears when the particles get into contact with each other. The tangential contact force reads

$$\mathbf{F}_{ct} = -\mu_k |\mathbf{F}_{cn} + \mathbf{F}_{adh}| \mathbf{t} \tag{4.18}$$

where μ_k is the coefficient of kinematic friction and $\mathbf{t}$ the unit vector in tangential direction. The adhesion force is given by

$$\mathbf{F}_{adh} = -\left| \frac{3}{2} \pi R_c \Gamma \right| \mathbf{n} \tag{4.19}$$

With Γ is the surface free energy between the interacting particles.

4.2 Numerical simulations

In this section the results of the numerical simulation are presented. With a simulation of a collision between two particles the energy transfer between the colliding particles is investigated. The influence of the impact position of the incident particle on the velocity ratio of the incident particle is investigated for different incident velocities and bed heights. The bed consist of nylon particles with a diameter of 5 millimetre and is stacked orthorhombic (see figure 4.3.a). The contact time of a steel incident particle colliding with a rectangular bed of steel particles (see figure 4.3.b) is also determined. The results of these numerical simulations are compared with the experimental results in the next section.

Figure 4.3: (a) Schematic representation of the orthorhombic bed of particles.
(b) Schematic representation of the rectangular bed of particles.

4.2.1 Two particle collision

When an incident particle collides with the bed particles energy transfer takes place. In the numerical model there should be preservation of energy during the collision, which means that the total energy that is put into the system should be equal to the energy at the end of the collision. For a collision between two nylon particles with a diameter of 5 mm, one with a incident speed that is smaller as the limiting elastic velocity and one with a higher velocity, is checked if there is energy preservation during the collision. The velocity at which only elastic deformation of the colliding particles occur is given by the limiting elastic velocity $v_{i,el}$. The limiting elastic velocity is given by [4]

$$v_{i,el} = \frac{\pi^2}{2\sqrt{10\rho_1}} \frac{y^{\frac{5}{2}}}{E^{*2}} \left(\frac{R_2}{R_1 + R_2} \right)^{\frac{3}{2}} \sqrt{\frac{1 + C_m}{C_m}} \tag{4.20}$$

In figure 4.4.a the deformation off two colliding particles as a function of the contact force is given for an elastic collision. In figure 4.4.b the deformation as a function off the contact force is given for an elastic-plastic collision.

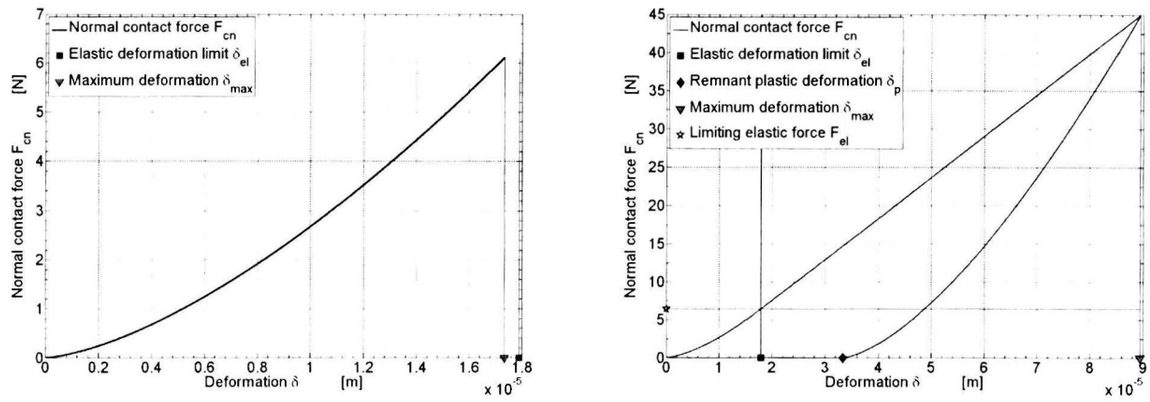

(a) (b)

Figure 4.4: Deformation of a two particle collision as function of the contact force.
(a) elastic collision with an incident speed $v_i = 1.5$ m/s,
(b) elastic-plastic collision with an incident speed $v_i = 10$ m/s.

In the case of an elastic collision the contact force increases to its maximum value in the approach phase and reduces to zero, along the same path, in the restitution phase. Because the collision is purely elastic there is no remnant plastic deformation of the particle. In the case of an impact speed that is higher then the elastic limiting velocity the collision becomes plastic-elastic. The particles start to deform elastically and when the deformation of the particle becomes larger than the elastic deformation limit plastic deformation starts until the maximum contact force is reached. In the restitution phase the contact force reduces to zero but not along the same path because energy is used to deform the colliding particles which leads to the remnant plastic deformation of the particles.

The energy content during the collision can be found by integrating the equation for the contact force and is equal to the surface area under the graph of the contact force (4.4.a and b). In figure 4.5.a the energy content in case of an elastic collision is shown and in figure 4.5.b in case of an elastic-plastic collision.

In the case of a purely elastic collision it can be seen that the kinetic energy is used to deform the colliding particles elastically until the relative speed of the two particles is zero, which results in a minimum in the kinetic energy and in a maximum in the elastic energy. In the restitution phase the stored elastic energy is released and the two particles are accelerated until the particles are not in contact anymore, which leads to the increase of the kinetic energy. In the case of an elastic-plastic collision the kinetic energy is also used to deform the colliding particle until there relative velocity is zero, but now a part of this energy is used for plastic deformation. The energy used for the plastic deformation is not given back to the particles which results in an lower kinetic energy content of the particles than at the start of the collision.

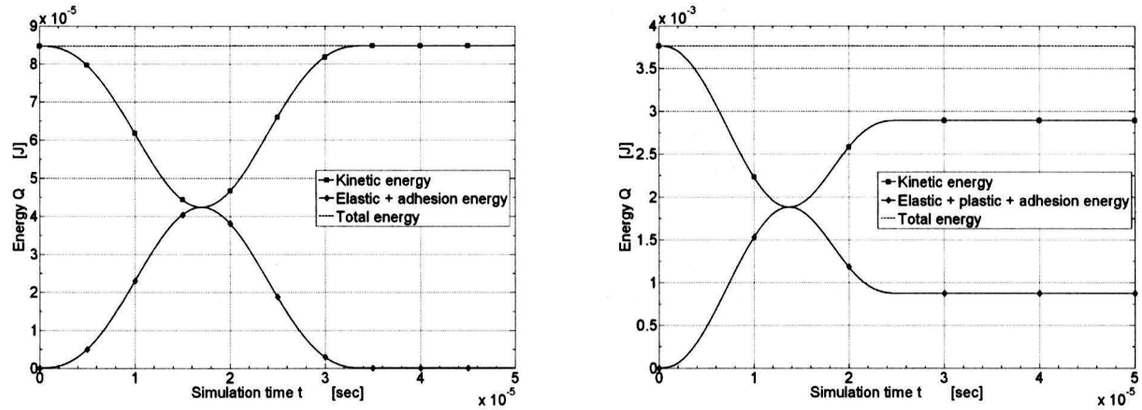

(a) (b)

Figure 4.5: Energy content during a two particle collision.
(a) elastic collision with an incident speed $v_i = 1.5$ m/s,
(b) elastic-plastic collision with an incident speed $v_i = 10$ m/s.

4.2.2 Steel particle colliding with a bed of nylon particles

The interaction of an incident particle with an orthorhombic bed of particles is simulated with the numerical code developed by Abd-Elhady [1, 2]. The code has been modified to take to perspex container into account in which the particles are situated during the experiments. In the numerical code the side walls of the perspex container are implemented. The diameter of the incident particle is the same as for the bed particles, namely 5 mm. The material of the bed particles is nylon and the material of the incident particle is steel. The bed consists of 42x1xn particles, with n the number of bed layers (9, 7, or 5 layers). The impact position of the incident particle is varied for three different impact angles α, as can been seen in figure 4.6. Where the impact angle α is defined as the angle between the center line of the colliding particles and the horizontal .

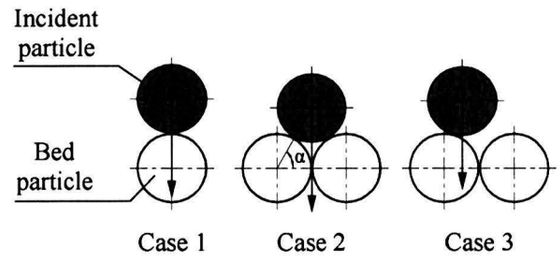

Figure 4.6: Definition of the impact positions and impact angle.

The impact angle for an impact corresponding with case 1 is 90 degrees, for case 2 60 degrees and for case 3 75 degrees. The incident velocity in the numerical calculations is varied between 1 and 8 m/s.

In figure 4.7 the particle motion of the incident particle and the bed particles is represented. The result of the numerical simulation is also included on the additional cd-rom (Figure-47.wmv). The impact position of the incident particle corresponds with case 1 and the incident velocity of the particle is 4.5 m/s and the time step between two successive pictures is 8 milliseconds. It can be seen that the particles in the top row near the impact position start to move upward in a triangular shape, with the incident particle as the top of the triangular shape. The target particle doesn't move as high as its two neighboring particles because the target particle is blocked by the incident particle after the collision. The target particle gives its energy back to the incident particle. There is also movement of the particles in the two layers below the impact point noticeable. The particles in this area don't move as high as the particles in the first layer. In the top row there is also some movement noticeable of a few particles that are situated further away from the impact point. In appendix G, and on the additional cd-rom (Figure-G1.wmv), the particle movement is presented of a collision with a steel incident particle hitting the bed with an impact angle of 75 degrees (case 3). The particle movement of this collision is almost the same as for an impact angle of 90 degrees. The biggest difference is the movement of the incident particle. The incident particle has a side way motion, because it hits the target particle off center. An other difference is the movement of the two neighboring particles of the target particle. The particle left of the target particle travels higher as the particle at the right of the target particle.

In order to see what happens on a smaller time scale with the dynamics of the particles the velocity vectors are plotted as a function of the simulation time. In figure 4.8 the velocity vectors of a collision are represented, whit a time step of 0.05 milliseconds.

The target particle starts to move downward immediately after impact of the incident particle. Because of the downward motion of the target particle the particles underneath the target particle start to move downward and some particles start to move to the side. Due to the motion of these particles a chain reaction is set in motion and other particles start to move downward and to the side. After 0.1 milliseconds the particles of the bottom layer start moving down and interact with the bottom. After interaction with the bottom the particles start to move up and forcing the particles above to move up.

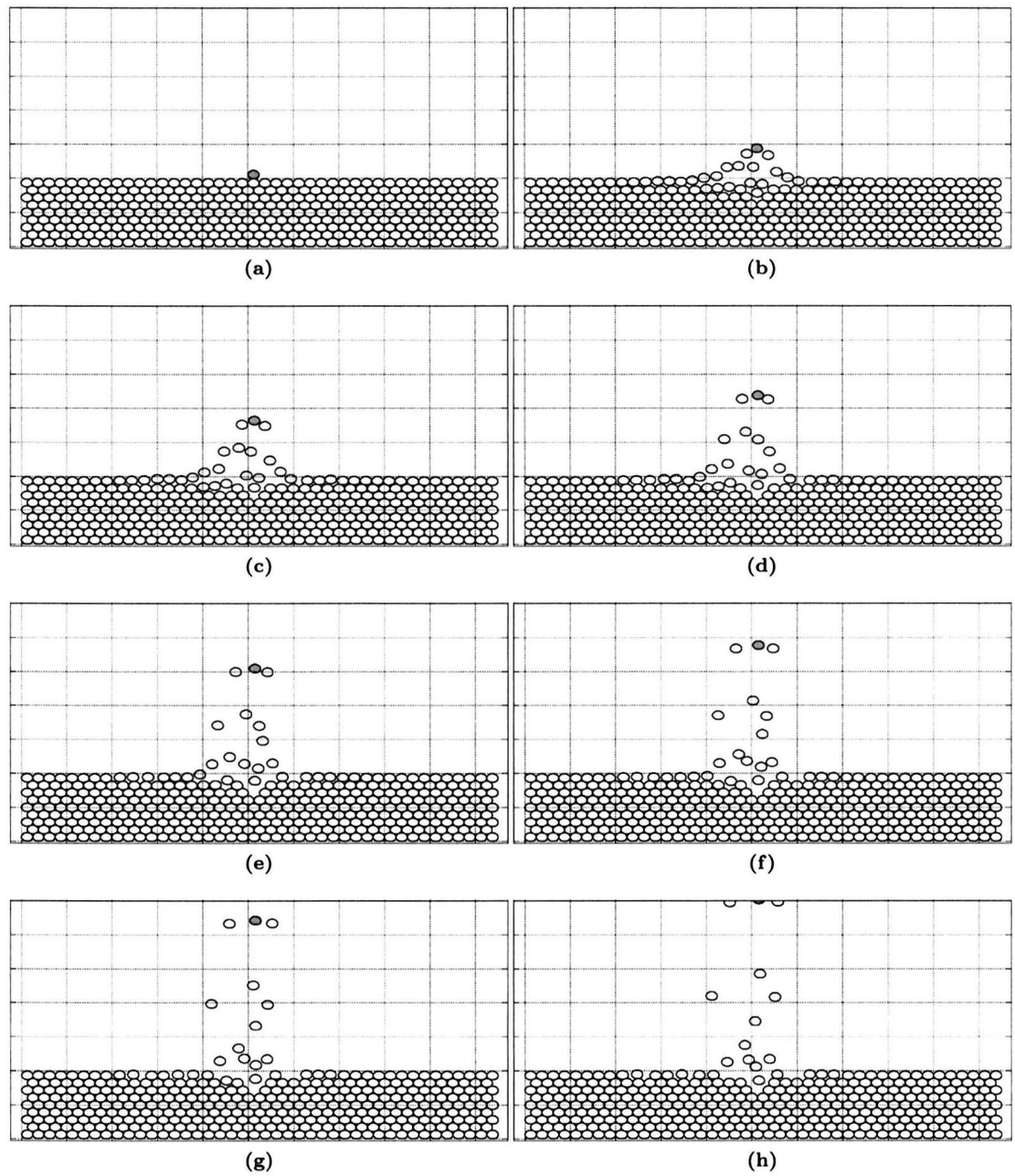

Figure 4.7: Particle movement of the incident particle and the bed particles after a collision with an impact angle of 90 degrees and a incident velocity of 4.5 m/s. Time step between two successive pictures is 8 ms.

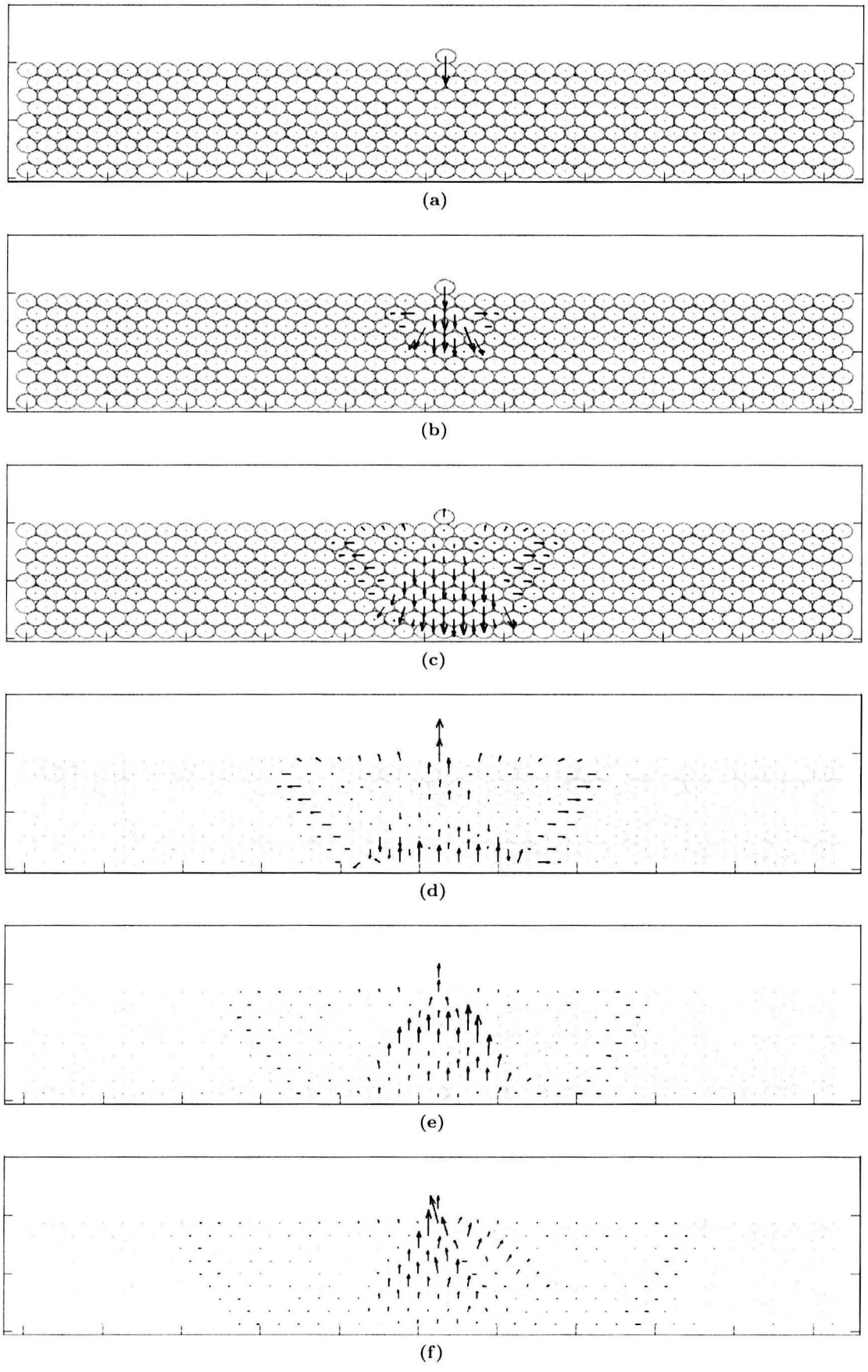

Figure 4.8: Velocity vector plot of a collision between a steel particle and a nylon bed collision. With an incident velocity of 4.5 m/s and an impact angle of 90 degrees. Time step between two successive pictures is 0.05 ms.

Influence of impact position

The velocity ratio of the incident particle is determined for several incident velocities and impact positions. The incident velocity is varied between 1 and 8 m/s for the three different impact positions (case 1, 2 and 3). The bed consists of 42x1x9 nylon particles. With the rebound velocity its possible to determine the velocity ratio of the incident particle. In figure 4.9 the velocity ratio is given as a function of the incident velocity for the three different impact positions.

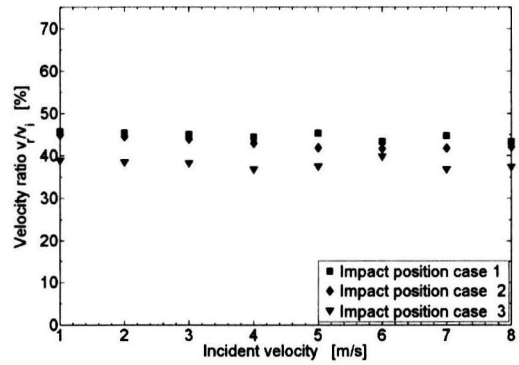

Figure 4.9: Rebound velocity as a function of the incident velocity for three impact positions.

The highest velocity ratio is found for an impact with an impact angle of ninety degrees. The velocity ratio for an impact position corresponding with case 1 is one or two percent higher than the velocity ratio for an impact position corresponding with case 2. For an impact in case 1 or 2 the energy transfer is symmetrical and therefor more energy is given back to the incident particle. When the impact position corresponds with case 3 the impact is not symmetrical and less energy is given back to the incident particle, which results in a lower velocity ratio. The velocity ratio for an impact corresponding with case 3 is approximately 8 percent lower.

Influence of the number of bed layers

The influence of the total number of bed layers on the velocity ratio is investigated for incident velocities ranging from 1 m/s to 8 m/s. The velocity ratio as a function of the incident velocity for different bed heights is given in figure 4.10.

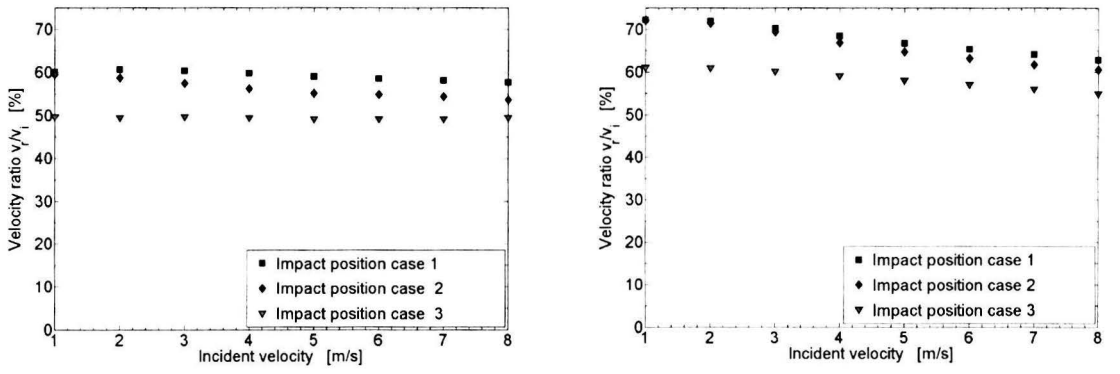

Figure 4.10: Rebound velocity as a function of the incident velocity for the three impact positions.
(a) For 7 bed layers.
(b) For 5 bed layers.

The velocity ratio increases with a decreasing amount of bed layers. For an impact corresponding with case 1 with an incident velocity of 1 m/s the velocity ratio is 46 percent for nine bed layers, 60 percent for seven bed layers and 72 percent for 5 bed layers. It is also found that the velocity ratio for an impact corresponding with case 2 is lower than the velocity ratio for an impact in case 1. The velocity ratio for an collision with an impact angle of 75 degrees (case 3) is lower than the velocity ratio for collisions corresponding to case 1 or 2, which is also found in the case of nine bed layers. The velocity ratio in the case of seven bed layers is 50 percent and 60 percent for five bed layers.

It can also be seen that the velocity ratio decreases with increasing incident velocity. In the case of seven bed layers the velocity ratio decreases from 60 to 57 percent and from 71 to 63 percent in the case of five bed layers, for a collision corresponding with case 1. The velocity ratio for case 2 follows the same trend. For a collision corresponding to case 3 the velocity ratio is round 50 percent for 7 bed layers and for 5 bed layers the velocity ratio decreases from 60 to 55 percent.

4.2.3 Steel particle colliding with a bed of steel particles

With the numerical program it is also possible to determine the contact time between the particles and the force propagation speed. The contact time and the force propagation speed are determined for a rectangular bed of steel (100Cr6) particles with a diameter of 20 mm (see figure 4.11 (a)). The incident particle is also a 20 mm steel particle and has an incident velocity of 2.7 m/s. In figure (4.11 b, c and d) the outcome of the calculations is given.

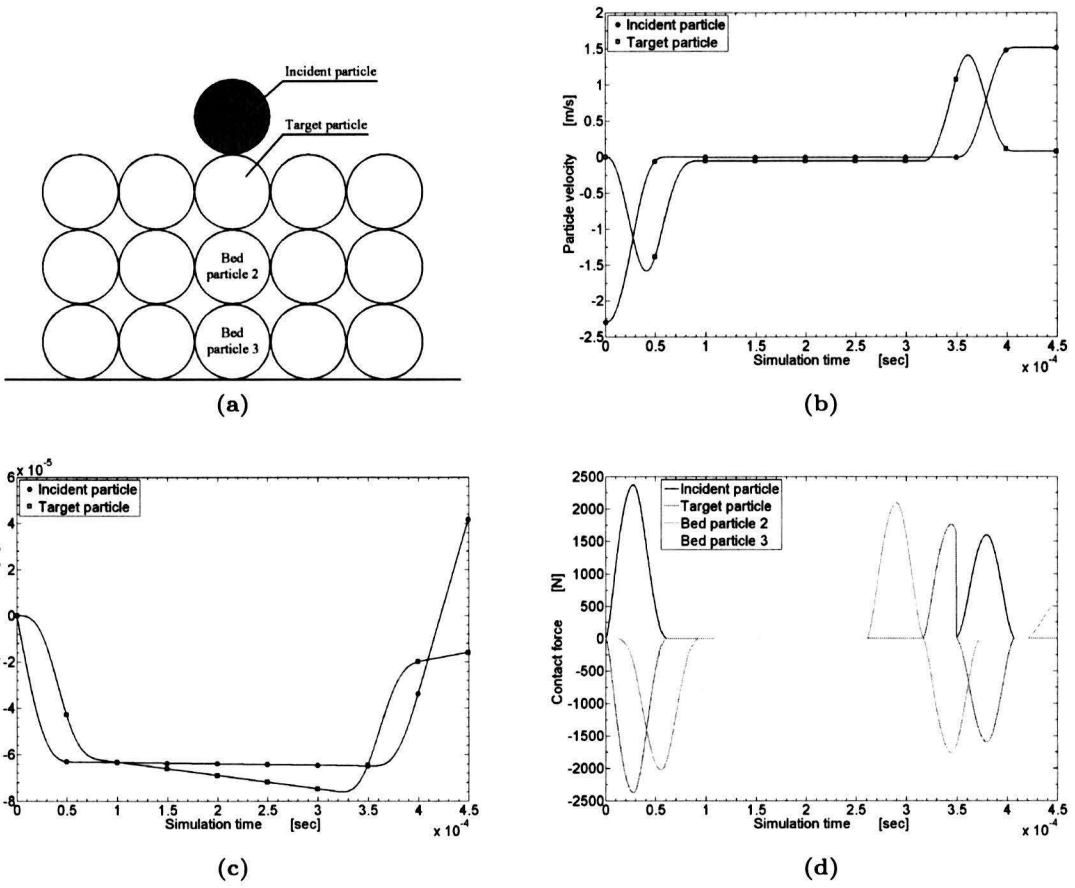

Figure 4.11: (a) Overview of the rectangular 5x1x3 bed.
(b) Particle velocity as a function of the simulation time.
(c) Particle displacement as a function of the simulation time.
(d) Contact force between interacting particles as a function of the simulation time.

The incident particle and the target particle are in contact with each other at the beginning of the numerical simulation. At the start of the collision the incident particle starts to move downward and deformation of the incident and target particle takes place. After 0.06 milliseconds the speed of the incident particle becomes zero and the contact with the target particle is broken. Between 0.06 and 0.34 milliseconds the downward movent of the target particle is only by gravity. After 0.09 milliseconds the velocity of the target particle becomes almost zero and the contact with bed particle 2 is lost.

After 0.32 milliseconds bed particle 2 starts to move upward and after 0.35 milliseconds the target collides with the incident particle and the incident particle starts to move upward. The incident particle starts to move upward 0.35 milliseconds after impact and after 0.42 milliseconds the incident particle reaches its original position. In figure 4.11 d the contact force as a function of the simulation time is given. The first time where the contact force in the target particle and bed particle 2 reaches its maximum is after 0.0255 respectively 0.056 milliseconds. The force propagation speed is determined by dividing the time difference between the first two maxima in the contact force by the particle diameter. The force propagation speed in this collision is 655 m/s.

4.3 Comparison between experimental and numerical results

Comparison of a steel particle hitting a nylon bed

In the 2D experiments with a steel incident particle colliding with a bed of nylon particles it is also found that the particles in the top row near the impact point start to move up in a triangular shape. The particles underneath the point of impact are also moving upward. The difference between the numerical calculation (figure 4.7) and the experiment (figure 3.15) is the amount of particles that move upward. In the experiment more particles, that are situated underneath the impact point, are moving upward as can be seen in figure 4.12.a and b. There is also upward movement of the particles in the upper layers of the bed, this is not found in the numerical simulation.

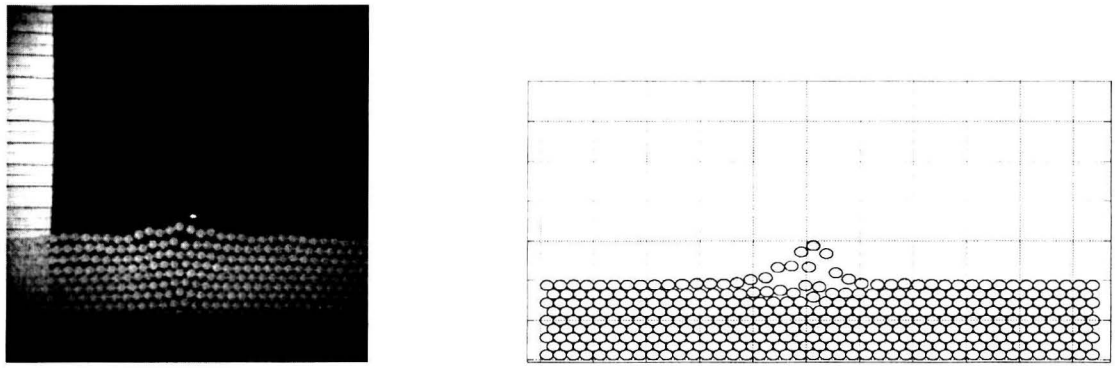

(a) (b)

Figure 4.12: Difference between the experimental and numerical particle motion.
(a) Particle motion found with an experiment (v_i = 4.5 m/s and t = 8 ms).
(b) Particle motion found with a numerical simulation (v_i = 4.5 m/s and t = 8 ms).

The different between the experiments and numerics could be explained by the use of compressed air to shoot the steel incident particle to the bed of nylon particles. When the steel particle is shot to the bed an air jet is traveling towards the bed. Most of the air reaches the bed way before the incident particle strikes the target particle. This air has no influence on the particle movement. But there is also an air column behind the steel particle and this air could influence the movement of the bed particles after impact of the incident particle. It could also be that the bed particles get an impuls from the perspex container.

In the experiments a lower velocity ratio for the incident particle is found in comparison to the numerical result, for the three different bed heights. The experimental results as well as the numerical results show that the velocity ratio increases with decreasing bed heights.

Comparison of a steel particle hitting a steel bed

In the 2D experiments with the 20 mm steel incident and bed particles the contact time is determined to be 0.404 milliseconds. In the numerical simulations the contact time is found to be 0.403 milliseconds. The contact time found with the numerical simulations corresponds with the experimental value. The time found for the target particle is lower in the numerical simulation than in the experiments, this could be explained by the friction between the bed particles. In the numerical simulation the collision is completely 2D, in the experiment the collision is not completely 2D. If the incident particle does not hit the target particle directly on top more friction between the bed particles is induced.

Chapter 5

Conclusions and recommendations

Conclusions

Impaction experiments were carried out in a 3D set-up in order to investigate the post-collision behavior of the incident particle and the bed particles. These experiments show that three different phenomena can occur during an impact of an incident particle on a bed of particles. The incident particle can stick to the bed or it can bounce off the bed. When the incident particle bounces off the bed, particles can be removed from the bed. The velocity at which removal occurs is found to be dependent on the diameter of the incident particle. With an increasing incident particle diameter, and a constant bed particle diameter, the removal velocity decreases. The velocities at which the post-collision phenomena take place show an overlap. This overlap in velocity regimes can be explained by several things. First of all the inhomogeneous bed due to the variation of the bed particle diameter. There is also an variation of the incident particle diameter.

Impaction experiments with the 2D set-up show that the velocity ratio of the incident particle is dependent on the impact position and the amount of bed layers. With a decreasing number of bed layers an increase in the velocity ratio is found. With a decreasing number of bed layers less particles are situated in the bed, so less energy is transferred to the bed particles. With the numerical simulations the influence of the impact position and number of bed heights is also found. The velocity ratio found in the numerical simulation is higher as the velocity ratio found in the experiments. In the numerical calculation the bed is completely 2D and in the experiments the bed is quasi 2D. Another influence in the experiments could be the influence of the air traveling behind the incident particle. In the experiments there could also be an influence of the spinning of the particles, which is not modeled in the numerical code.

The contact time measured in the experiments corresponds with the contact time found with the numerical code. With the use of bigger steel particles the influence of the air is much smaller because the mass of the particles is much higher.

Recommendations

During the experiments a lot of effort is made to exclude the influence of the compressed air on the outcome of the 2D experiments. However there is always an air jet traveling behind the incident particle that could influence the outcome of the collision, therefor it is advisable to fabricate a mechanical shooting mechanism that does not use compressed air. The shooting mechanism could be equipped with a spring mechanism.

It is also advisable to equip the experimental set-up with a triggering system that starts the high speed camera at the same time when the incident particle is released from the shooting mechanism. This is especially convenient in the case of short recording times (high frame rates) for instance in the case of measuring the contact time between the colliding particles.

With the 2D experiments a big influence of the bottom wall on the particle motion is found. The influence of the bottom wall on the outcome of the collision needs to be further investigated experimentally and numerically. In the experiments the perspex bottom wall could be varied in thickness or the material itself could be changed.

Bibliography

[1] Abd-Elhady, M.S., Gas-side particulate fouling in biomass gasifiers , *PhD Thesis*, Eindhoven University of Technology, The Netherlands, 2005.

[2] Abd-Elhady, M.S., Rindt, C.C.M., Wijers, J.G. and Steenhoven van, A.A., Modelling the impaction of a micron particle with a powdery layer, *Powder Technology*, vol. 168 (3), pp. 111-124, 2006.

[3] Abd-Elhady, M.S., Gäbler, J., Rindt, C.C.M. and Steenhoven van, A.A., Crititcal penetration velocity for particulate fouling layers, *in Proceedings 13th International Heat Transfer Conference*, FOU01, 2006

[4] Beek van, M.C., Gas-side fouling in heat-recovery boilers, *PhD thesis*, Eindhoven University of Technology, The Netherlands, 2001.

[5] Clevers, S.H., Influence of sintering on the fouling mechanism, *Thesis*, Eindhoven University of Technology, The Netherlands, 2004.

[6] Duran, J., *Sands, powders and grains; an introduction to the physics of granular materials*, Springer, 2000.

[7] Heldens, J.P., Ontwerp van een experimentele opstelling, *WET 2006.07*, Eindhoven University of Technology, The Netherlands, 2006.

[8] International Energy Agency, *World Energy Outlook 2006*, International Energy Agency, 2006.

[9] Johnson, K.L., *Contact mechanics*, Cambridge University Press, 1985.

[10] Johnson, K.L., Kendall, K. and Roberts, A.D., Surface energy and the contact of elastic solids, *Proceedings Royal Society A*, vol. 324, pp. 301-313, 1971.

[11] Nishida, M., Tanaka, K. and Mutsumoto, Y., Discerete element method simulation of the restitutive characteristics of a steel spherical projectile from a particulate aggregation, *JSME International Journal*, vol. 47 (3), pp. 438-447, 2004.

[12] Tanaka, K., Nishida, M., Kunimochi, T. and Takagi, T., Discrete element simulation and experiment for dynamic response of two-dimensional granular matter to the impact of a spherical projectile, *Powder Technology*, vol. 124 (1-2), pp. 160-173, 2002.

[13] Thornton, C. and Ning, Z., A theoretical model for the stick/bounce behavior of adhesive, elastic-plastic spheres, *Powder Technology*, vol. 99 (2), pp. 154-162, 1998.

[14] Tsuji, Y., Kawaguchi, T. and Tanaka, T., Discrete particle simulation of two-dimensional fluidized bed, Powder Technology, vol. 77, pp. 79-87, 1993.

[15] Wolffs, S.U.N., 2D-botsingsopstelling, *WET 2006.17*, Eindhoven University of Technology, The Netherlands, 2006.

[16] Makin metal powders, www.makin-metals.com

[17] Hoover precision, www.hooverprecision.com

[18] Polymer data handbook, Oxford University Press, www3.oup-usa.org/pdh/

[19] Imagetool, http://ddsdx.uthscsa.edu/dig/download.html

Appendix A

Energies involved in a two-body collision

In this appendix the different energies for the two-body collision model [4] are presented.

Elastic impact

In the two-body collision model the maximum contact force between the interacting particles is calculated by solving the energy balance that holds at the end of the approach phase. In the case of a purely elastic collision the energy balance is given as [4]

$$Q_k + Q_{A,a}(F) = Q_e(F) \tag{A.1}$$

The kinetic energy Q_k is the kinetic energy of the incident particle with an effective mass m^* and is given as

$$Q_k = \frac{1}{2} m^* v_i^2 \tag{A.2}$$

The surface energy $Q_{A,a}$ is given as

$$Q_{A,a} = \Gamma\pi \left(\frac{R^* F}{\frac{4}{3} E^*} \right)^{\frac{2}{3}} \tag{A.3}$$

with Γ the work of adhesion and is given by $\Gamma = 2\sqrt{\gamma_1 \gamma_2}$. The net adhesion energy $Q_{A,r} - Q_{A,a}$ is given as

$$Q_{A,r} - Q_{A,a} = 7.09 \left(\frac{R_c^4 \Gamma^5}{E^{*2}} \right)^{\frac{1}{3}} \tag{A.4}$$

with R_c is the contact radius and which is equal to R^* in the case of an elastic collision.

The elastic energy Q_e stored in the colliding particles is given by the integral of the contact force F over the distance between the limits 0 and δ. The contact force is given by the Hertz equation as

$$F = \frac{4}{3} E^* R^{*\frac{1}{2}} \delta^{\frac{3}{2}} \tag{A.5}$$

Integration of the Hertz equation leads to the elastic energy and reads

$$Q_e = \int_0^{\delta} F \mathrm{d}\delta = \frac{2}{5} \frac{F^{\frac{5}{3}}}{\left(\frac{4}{3} E^*\right)^{\frac{2}{3}} R^{*\frac{1}{3}}} \tag{A.6}$$

Elastic-plastic impact

In the case of an elastic-plastic collision the energy balance is given as [4]

$$Q_k + Q_{A,a}(F) = Q_{el} + Q_{pe}(F) + Q_p(F) \tag{A.7}$$

The surface energy in the approach phase of an elastic-plastic impact can be written as

$$Q_{A,a} = \Gamma \pi \left(\left(\frac{\pi R^*}{2E^*} y \right)^2 + \frac{F - F_{el}}{\pi y} \right) \tag{A.8}$$

The amount of elastic energy in an elastic-plastic collision is limited by the elastic deformation limit δ_{el} and reads

$$\delta_{el} = \left(\frac{2}{3} \pi \right)^2 \frac{R^*}{\left(\frac{4}{3} E^*\right)^2} y^2 \tag{A.9}$$

Substituting the elastic deformation limit in the Hertz equation leads to the limiting elastic force F_{el}. The elastic energy in an elastic-plastic collision than reads

$$Q_{el} = \frac{2}{5} \left(\frac{2}{3} \right)^5 \frac{\pi^5 R^{*3}}{\left(\frac{4}{3} E^*\right)^4} y^5 \tag{A.10}$$

During the plastic deformation of the particles also elastic deformation takes place the elastic energy Q_{pe} during plastic deformation is given as

$$Q_{pe} = \frac{1}{2} \delta_{el} (F - F_{el}) \tag{A.11}$$

The dissipated energy required to give the contact a remnant deformation H can be calculated from the integral of the plastic force component F_p between the limits 0 and H. The remnant deformation can be written as $H = \delta - \delta_{el}$ and the plastic force component F_p as $F_p = \pi y R^* (\delta - \delta_{el})$ [1, 10]. The dissipated energy becomes

$$Q_p = \int_0^{H} F_p \mathrm{d}H = \frac{(F - F_{el})^2}{2\pi R^* y} \tag{A.12}$$

Appendix B

The coefficient of restitution for the spring-damper model

The equation of motion for the spring-damper model [12] is given as

$$m\ddot{\mathbf{x}} + \eta\dot{\mathbf{x}} + K\mathbf{x} = 0 \tag{B.1}$$

with K the spring coefficient and η the damping coefficient. Rearranging the equation and making use of the definition of the eigen frequency ω_0 and damping ratio γ leads to

$$\ddot{\mathbf{x}} + 2\gamma\omega_0\dot{\mathbf{x}} + \omega_0^2\mathbf{x} = 0 \tag{B.2}$$

with ω_0 defined as $\omega_0 = \sqrt{\frac{K}{m}}$ and γ defined as $\gamma = \frac{\eta}{2\sqrt{Km}}$. The solution of this equation, at the initial conditions $\mathbf{x}_{(t=0)} = 0$ and $\dot{\mathbf{x}}_{(t=0)} = v_i$, is given as

$$\mathbf{x} = \left(\frac{v_i}{q}\right)\sin(qt)\exp(-\gamma\omega_0 t) \tag{B.3}$$

$$\dot{\mathbf{x}} = \left(\frac{v_i}{q}\right)\exp(-\gamma\omega_0 t)(q\cos(qt) - \gamma\omega_0\sin(qt)) \tag{B.4}$$

with q defined as $q = \omega_0\sqrt{1-\gamma^2}$. The oscillation period of this system is $2\pi/q$. The contact of two particles starts at time $t = 0$ and ends at time $t = \pi/q$. So the rebound velocity at the time $t = \pi/q$ is given as

$$v_r = \dot{\mathbf{x}}|_{t=\pi/q} = -v_i\exp(-\gamma\omega_0\pi/q) \tag{B.5}$$

The coefficient of restitution is defined as the ratio between the rebound velocity and the incident velocity and reads

$$e = -\frac{v_r}{v_i} = \exp(-\gamma\omega_0\pi/q) \tag{B.6}$$

The coefficient of restitution in the spring-damper model appears to be constant and therefore independent of the incident velocity.

Appendix C

Material properties

Table C.1: Material properties bronze particles.

Property		Bronze
Young's modulus E	[N/m^2]	1.29x10^{11}
Yield stress σ_y	[N/m^2]	3.0x10^8
Density ρ	[kg/m^3]	1.18x10^3
Surface free energy γ	[mJ/m^2]	-
Poison ratio ν	[-]	0.35
Friction coefficient μ	[-]	-

Table C.2: Material properties used in simulations.

Property		Steel	Steel (100Cr6)	Nylon	Perspex
Diameter d	[m]	5x10^{-3}	20x10^{-3}	5x10^{-3}	-
Young's modulus E	[N/m^2]	2.15x10^{11}	2.15x10^{11}	3.20x10^9	3.25x10^9
Yield stress σ_y	[N/m^2]	2.0x10^9	2.60x10^9	86.0x10^6	76.0x10^6
Density ρ	[kg/m^3]	7.81x10^3	7.87x10^3	1.15x10^3	1.18x10^3
Surface free energy γ	[J/m^2]	0.16	0.16	0.04	0.04
Poison ratio ν	[-]	0.28	0.28	0.33	0.35
Friction coefficient μ	[-]	0.2	0.2	0.15	0.15

Appendix D

Data impaction experiments micron particles

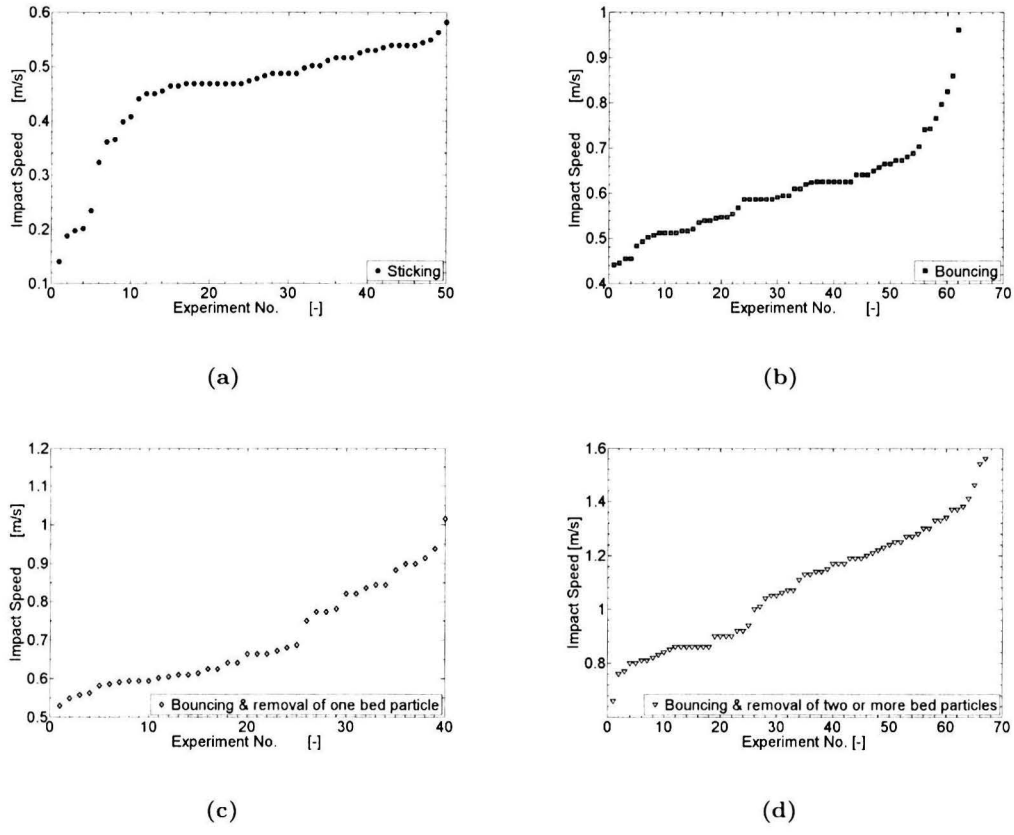

Figure D.1: Post-collision behavior of an incident particle (d = 52 μm) as a function of the vertical impact speed.
(a) Sticking of the incident particle. (b) Bouncing of the incident particle.
(c) Removal of one bed particle. (d) Removal of two or more bed particles.

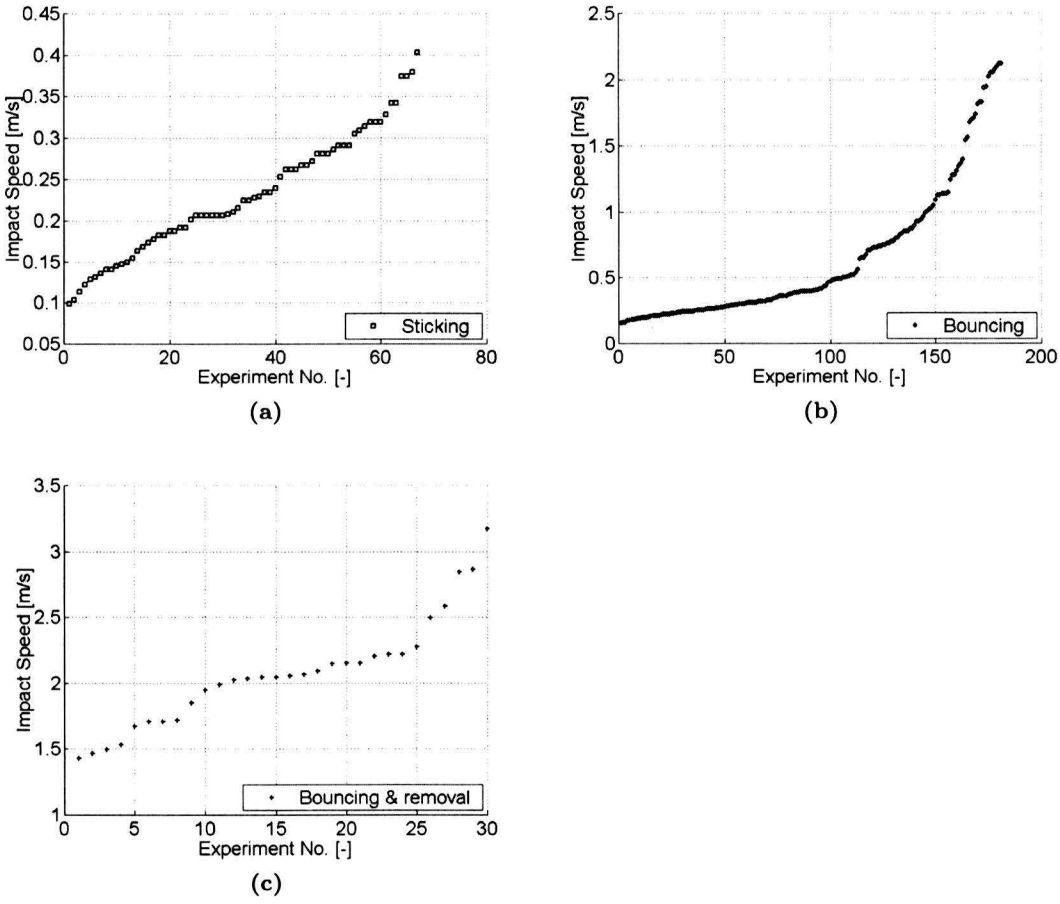

Figure D.2: Post-collision behavior of an incident particle (d = 75 μm) as a function of the vertical impact speed.
(a) Sticking of the incident particle. (b) Bouncing of the incident particle.
(c) Removal of bed particles.

Appendix E

Experimental results 2D impaction experiments

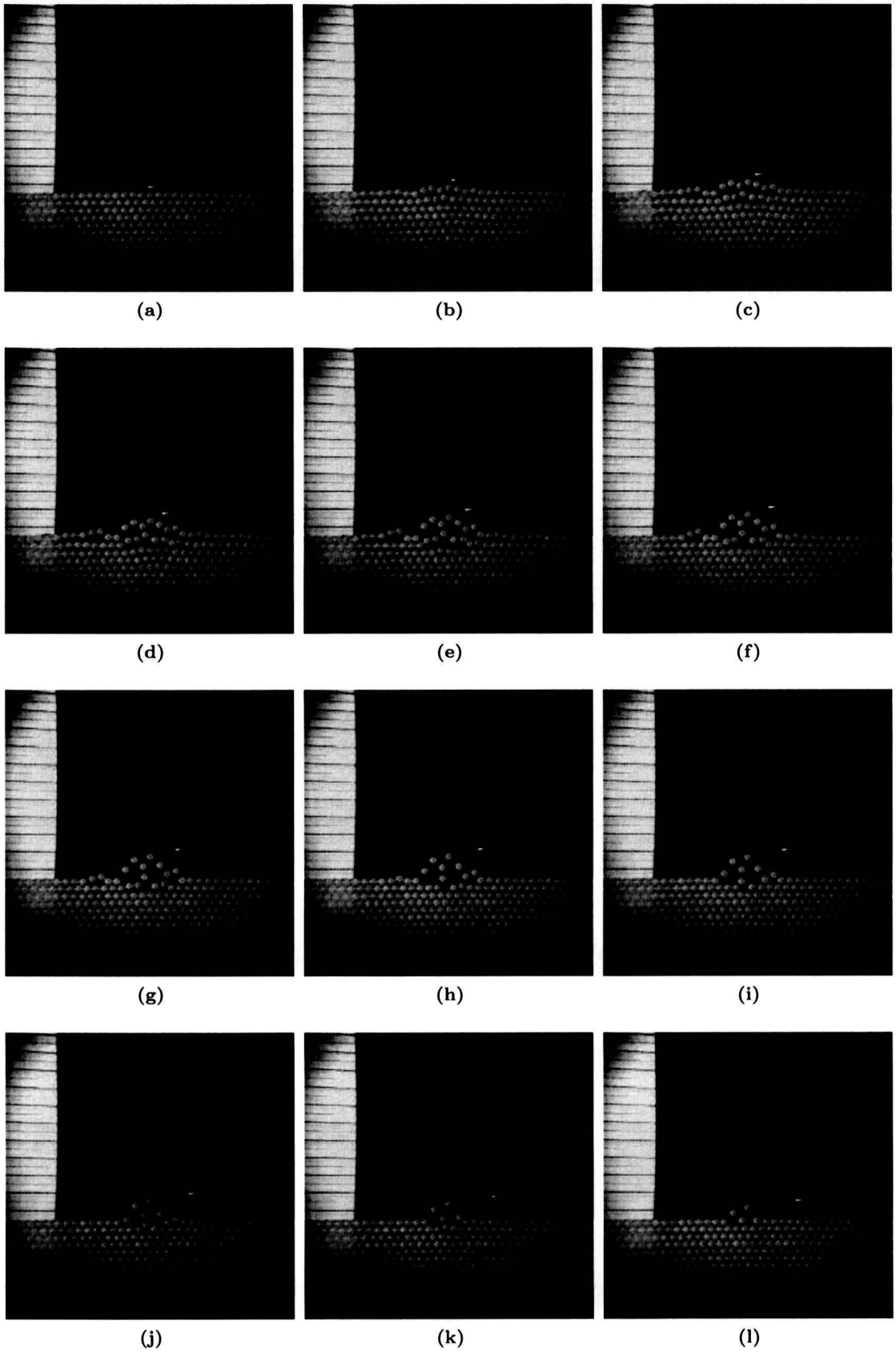

Figure E.1: Collision of a steel particle on a nylon bed of particles with an impact speed of 2.6 m/s. Time step between two successive pictures is 8 ms.

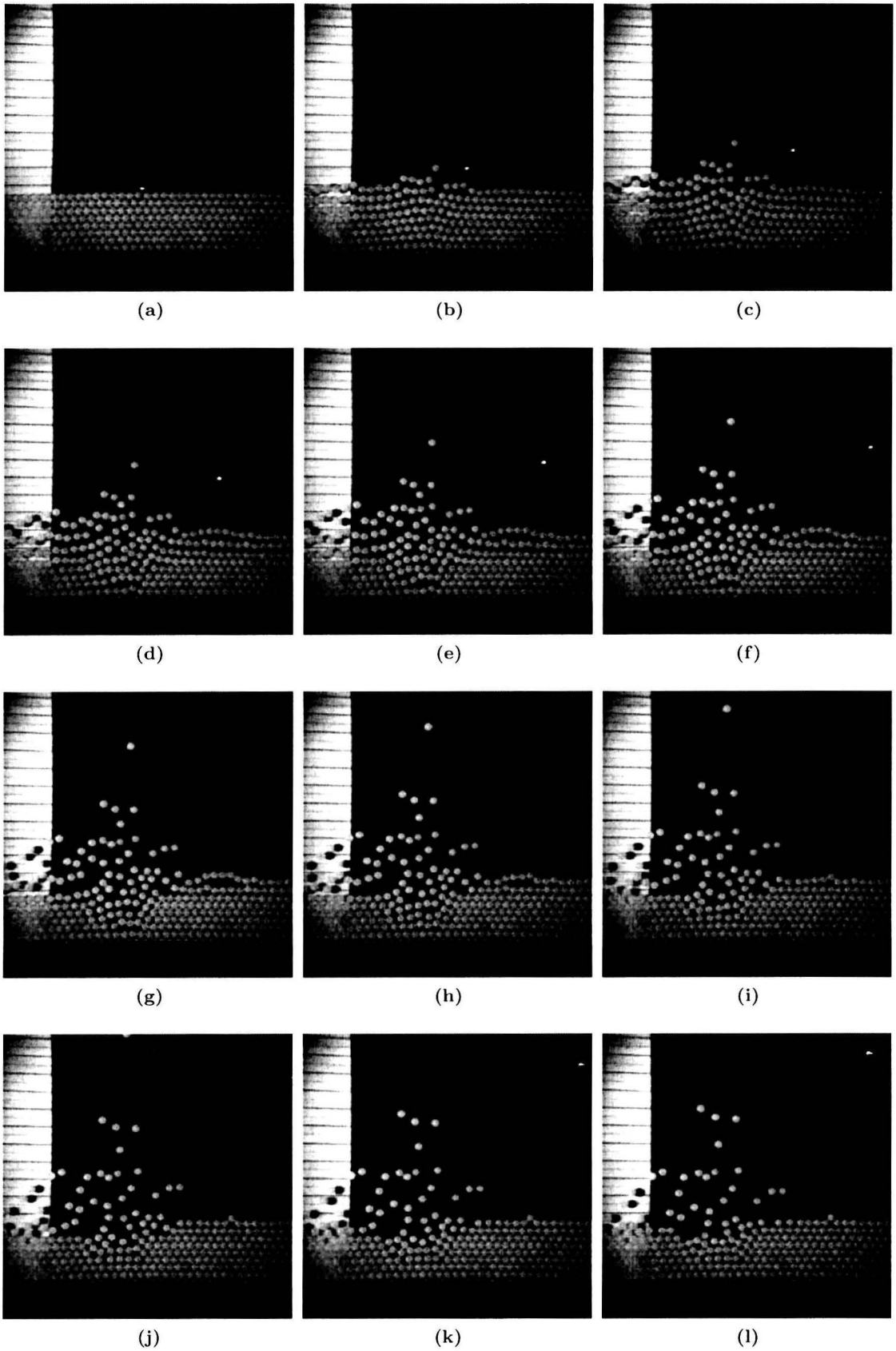

Figure E.2: Collision of a steel particle on a nylon bed of particles with an impact speed of 7.5 m/s. Time step between two successive pictures is 8 ms.

Appendix F

Experimental results Tanaka

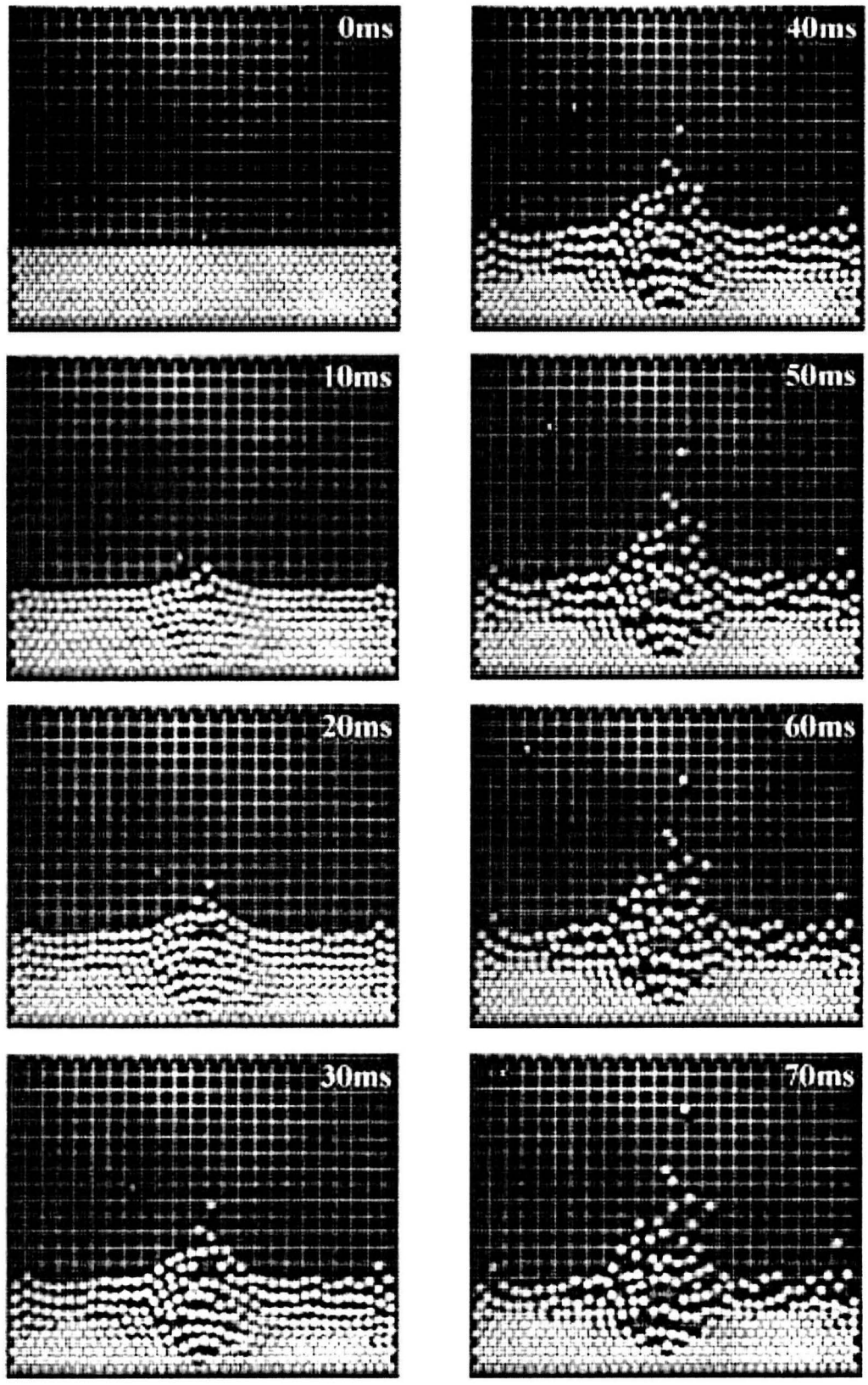

Figure F.1: Motion of spheres in the rectangular arrangement taken by a high-speed video camera: the impact velocity is 8.9 m/s.

Appendix G

Numerical results

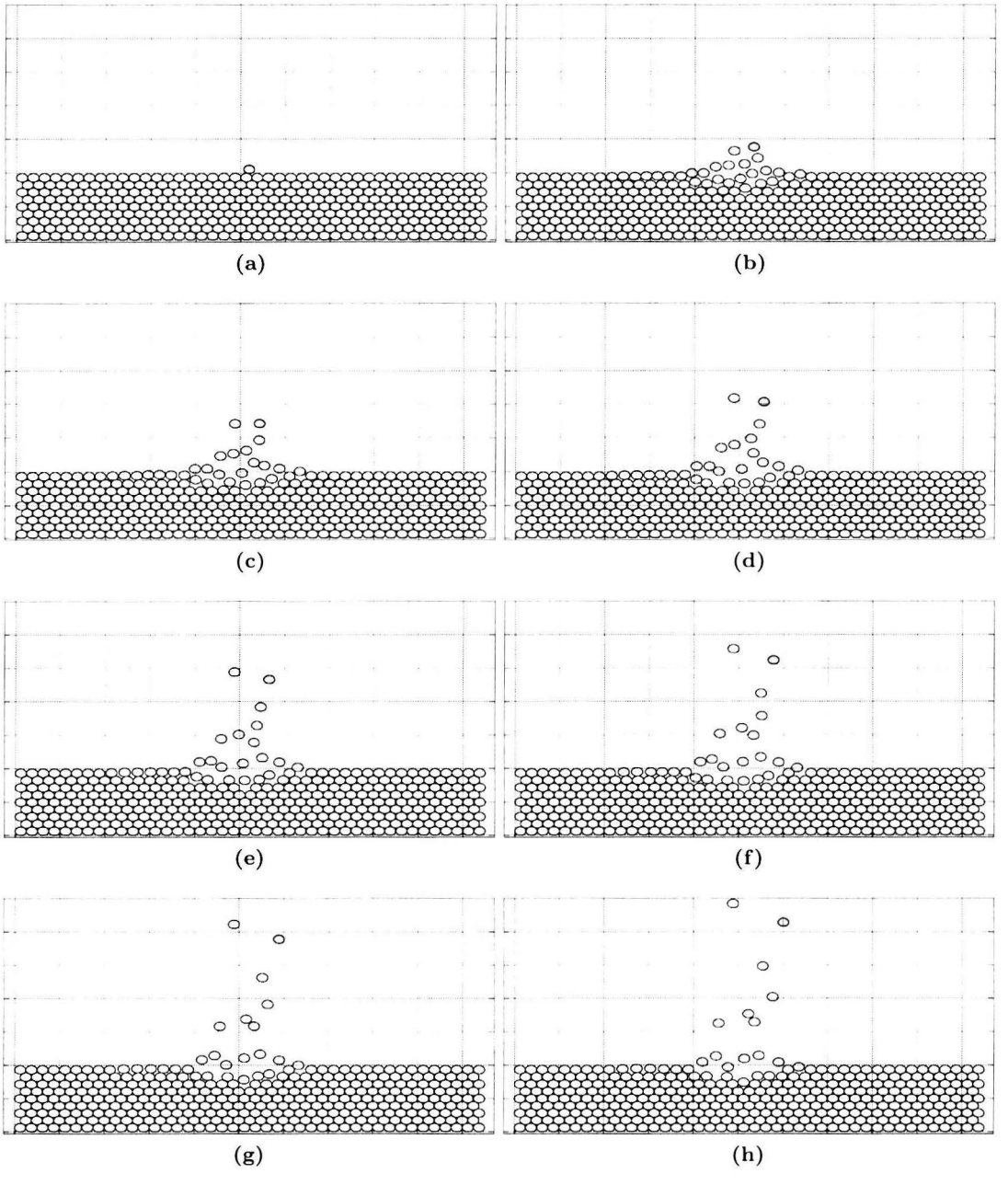

Figure G.1: Collision of a steel particle on a nylon bed of particles with an impact speed of 4.5 m/s. Time step between two successive pictures is 8 ms.